Applications of piezoresponse force microscopy in materials research: from inorganic ferroelectrics to biopiezoelectrics and beyond

D. Denning[1,2], J. Guyonnet[1,2,*], and B. J. Rodriguez[1,2,*]

[1]Conway Institute of Biomolecular and Biomedical Research, University College Dublin, Belfield, Dublin 4, Ireland
[2]School of Physics, University College Dublin, Belfield, Dublin 4, Ireland
[*]Corresponding authors email addresses: jill.guyonnet@ucd.ie, brian.rodriguez@ucd.ie

Abstract

Piezoresponse force microscopy (PFM) probes the mechanical deformation of a sample in response to an electric field applied with the tip of an atomic force microscope. Originally developed more than two decades ago to study ferroelectric materials, this technique has since been used to probe electromechanical functionality in a wide range of piezoelectric materials including organic and biological systems. PFM has also been demonstrated as a useful tool to detect mechanical strain originating from electrical phenomena in nonpiezoelectric materials. Paralleling advances in analytical and numerical modelling, many technical improvements have been made in the last decade: switching spectroscopy PFM allows the polarisation switching properties of ferroelectrics to be resolved in real space with nanometric resolution, while dual ac resonance tracking and band excitation PFM have been used to improve the signal-to-noise ratio. In turn, these advances have led to increasingly large multidimensional data sets containing more complete information on the properties of the sample studied. In this review, PFM operation and calibration are described, and recent advances in the characterisation of electromechanical coupling using PFM are presented. The breadth of the systems covered highlights the versatility and wide applicability of PFM in fields as diverse as materials engineering and nanomedicine. In each of these fields, combining PFM with complementary techniques is key to develop future insight into the intrinsic properties of the materials as well as for device applications.

1 Introduction

Electromechanical coupling in piezoelectric and ferroelectric materials has been studied at the macroscopic scale via a range of techniques including quasistatic meter, charge amplifiers, double-beam laser interferometry, and ultrasound interference.[1] In parallel, the ability to grow single-crystalline materials allowed these macroscopic properties to be correlated to their crystal structure.[2] Modern technological advances, however, make increasing use of materials properties at the micro- and nanoscale, with samples in composite, polycrystalline, semiconducting, and thin film form.[3] In such samples, the macroscopic mechanical, dielectric, and piezoelectric properties can be affected by the micro- to nanoscopic disordered structure. Two examples are polycrystalline piezoelectric materials, whose net piezoelectric effect measured at the macroscale is typically reduced due to the different contributions from randomly oriented nano- to microscopic grains,[4] and ferroelectrics, where nanoscale domains of variously orientated polarisation affect the dielectric susceptibility[5] and piezoelectric response.[6,7] In this context, the advent of atomic force microscopy (AFM) techniques and their ability to probe matter with nanometric lateral resolution has allowed the physical limits of electromechanical phenomena to be explored.[8–12]

AFM has been instrumental in ushering in the age of nanotechnology owing to its high resolution and sensitivity across a range of interaction forces, allowing AFM to find applications in materials science, physics, chemistry, and biology.[13] Initially developed to map surface topography of materials,[14]

various modalities were subsequently developed to probe, e.g., mechanical, magnetic, electrical, and chemical properties.[15–21] Piezoresponse force microscopy (PFM)[22,23] and, more recently, the related electrochemical strain microscopy (ESM)[24,25] have been used as local probes of electromechanical and electrochemical coupling, respectively. PFM was first demonstrated in 1992 to probe local coupling between an electrically-biased probe and a resulting mechanical sample deformation in a ferroelectric polymer,[26] following related approaches to study local piezoelectricity using scanning acoustic[27] and scanning tunneling microscopy.[28] Shortly thereafter, several groups were using PFM to investigate inorganic ferroelectric materials.[29–38]

PFM has been key to advancing our understanding of ferroelectric materials and optimising their performance for an increasingly vast range of applications, including nonvolatile ferroelectric random access memory (FeRAM) devices,[39,40] memristive behaviour in ferroelectric tunnel junctions,[41] and enhancing the efficiency of solar cells.[42,43] Perovskite materials specifically designed for solar cell devices have also been investigated using PFM.[44] In parallel, ESM has become a powerful tool for probing electrochemistry and ionic transport in solid materials, with applications in energy storage devices.[24,25] The success and longevity of these techniques relate to their usefulness for the investigation of structure-property relationships for a wide variety of materials spanning from traditional inorganic ferroelectric films, crystals, and nanostructures, to organic ferroelectric polymers, piezoelectric semiconductors, piezoelectric biomaterials, and, more recently, to nonpiezoelectric materials, including Li-ion battery cathodes. The robustness of PFM combined with the ubiquity of various forms of electromechanical coupling across a range of materials systems have raised PFM and related techniques from a niche application to a standard mode of most commercial AFM systems. Furthermore, PFM-related research has recently been promoted and recognised by a series of international symposia and workshops and regular special issues in the *Journal of Applied Physics*.[45–47]

This review is meant to complement existing reviews addressing PFM[17,48–60] by providing an overview of the technique and practical guidelines for implementation, while highlighting the breadth of materials studied by PFM.

2 Principles of piezoresponse force microscopy

2.1 Experimental details

2.1.1 Essentials of PFM

In PFM, a conductive (often metal-coated) AFM tip is brought into contact with the surface of a sample, thus acting as a sharp top electrode, while the other side of the sample is connected to a grounded bottom electrode. A voltage is applied to the tip (or, in some cases, to the bottom electrode while the tip is grounded):

$$V_{tip} = V_{dc} + V_{ac} \cdot \cos(\omega t), \tag{1}$$

where ω is the chosen modulation frequency and V_{dc} is an optional dc offset. If the sample is piezoelectric, the surface of the sample deforms mechanically in response to the applied voltage due to the converse piezoelectric effect. The position of the sample surface, u, is given by

$$u = u_0 + \Delta_u \cdot \cos(\omega t + \varphi), \tag{2}$$

where u_0 is the equilibrium position, Δ_u is the amplitude of deformation, and φ is the phase difference between the excitation signal and the resulting oscillatory deformations. u is detected via the motion of the cantilever, monitored by optical beam deflection AFM. Formally, the piezoresponse is defined as the first harmonic component of the tip oscillation:

$$A_{1\omega} = A \cdot \cos(\omega t + \varphi), \tag{3}$$

where A is the oscillation amplitude, given in units of length. In practice, A is tracked by recording the position-sensitive detector (PSD) signal, which is input in a lock-in amplifier (LIA) with the excitation signal as reference. The demodulated signal is

$$R_{1\omega} = R \cdot \cos(\omega t + \varphi), \tag{4}$$

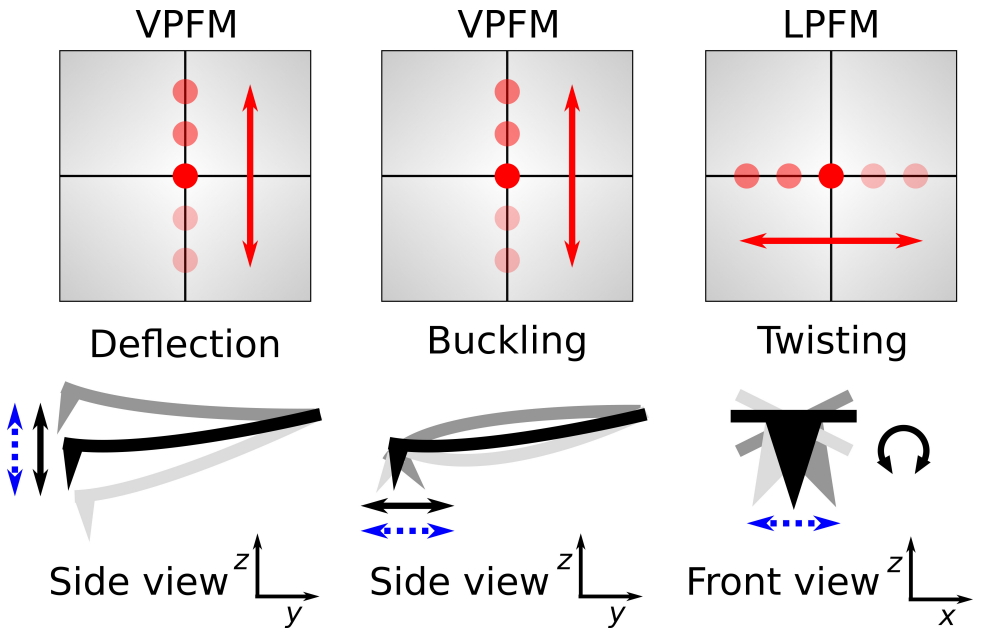

Figure 1: Illustration of possible cantilever motions in PFM. Flexural deflection (left), detected in VPFM, originates from an out-of-plane piezoresponse. Flexural buckling (centre), detected in VPFM, and lateral twisting (right), detected in LPFM, both originate from an in-plane piezoresponse. The double arrows in the upper part of the figure represent changes in the laser spot position on the PSD. The solid double arrows in the lower part represent the cantilever motion, while the dashed double arrows represent the motion of the sample surface acting of the cantilever.

where the amplitude, R, has units of Volts. It follows that

$$R_{1\omega} = \alpha \cdot A_{1\omega}, \tag{5}$$

where α is a calibration parameter, measured in Volts per meters, that depends on the optical sensitivity and the LIA parameters. With adequate calibration of the setup, R and φ thus give quantitative information about the magnitude and orientation of the surface deformations, respectively. This is further discussed in Sect. 2.1.2. The LIA can also output the signal as mixed components, $X = R{\cdot}\sin(\varphi)$ and $Y = R \cdot \cos(\varphi)$. When using this vector representation, the phase reference of the LIA is usually adjusted (on a single data point) so that X is maximised. While direct data interpretation is less straightforward in this case because the amplitude and phase are both contained in one signal, this method allows the effects of instrumental offsets to be minimised.[60]

PFM can measure both out-of-plane and in-plane components of the piezoresponse, allowing so-called vector PFM.[53] This is achieved by performing complementary measurements referred to as vertical PFM (VPFM) and lateral PFM (LPFM). As illustrated in Fig. 1, VPFM detects vertical movements of the laser position on the PSD, associated with the flexural deflection or buckling of the cantilever, while LPFM detects the lateral movements of the laser position, associated with the lateral twisting of the cantilever. Importantly, flexural deflection is caused by an out-of-plane piezoresponse (deformations in the z direction), but flexural buckling is caused by an in-plane piezoresponse parallel to the cantilever axis (deformations in the y direction). Lateral twisting is caused by an in-plane piezoresponse perpendicular to the cantilever axis (deformations in the x direction). Therefore, two distinct contributions (deflection and buckling) can be present in the VPFM signal, and LPFM depends on the angle of the cantilever in the plane of the sample surface with respect to the in-plane piezoresponse orientation. For these reasons, it is often necessary to perform measurements at different cantilever angles in order to clearly distinguish the different contributions. This is further discussed in Sect. 2.3.3.

2.1.2 Requirements for quantitative PFM

The amplitude of deformation at the surface of the sample due to the converse piezoelectric effect, Δ_u, is a linear function of the applied PFM voltage as

$$\Delta_u = d_{ij} \cdot V_{ac}, \tag{6}$$

where d_{ij} is the local relevant element of the third-rank d_{ijk} piezoelectric tensor of the material, measured in units of length per volt.[61] In theory, a quantitative measure of d_{ij} is therefore possible, assuming the electric field produced by V_{ac} is homogeneneous in the z direction and that Δ_u accurately represents the piezoresponse amplitude, A. Although the first condition is usually met, the presence of a contamination layer on the sample surface (or tip) can however reduce the effective applied voltage. The second condition represents a longstanding challenge in quantitative PFM. First, although only electromechanical contributions should ideally be detected in A, there can exist other physical contributions: long-range electrostatic interactions and nonlocal interactions between the tip and the sample surface can contribute to the total amplitude, such that $A = A_{piezo} + A_{el} + A_{nl}$, where A_{piezo}, A_{el}, and A_{nl} are the piezoelectric, electrostatic, and nonlocal contributions, respectively.[62] A number of approaches have been developped for minimising A_{el} and A_{nl}, as further discussed in Sect. 2.3.1. Secondly, the effects of the cantilever dynamics on the optical beam deflection system can pose a challenge, as the detection of the cantilever deflection depends on the position of the laser spot on the back of the cantilever and is therefore an indirect measurement of Δ_u. Labuda and Proksch[63] recently quantified this effect in a comparative study using conventional beam deflection and laser Doppler vibrometry, where the latter method directly detects Δ_u and can be positioned very accurately due to the small laser spot size. Important effects were observed on both the phase and amplitude of the piezoresponse, affecting the reproducibility of d_{ij} measurements and ferroelectric domain imaging. The latter are further discussed in Sect. 3.2.

In the ideal case where $A = A_{piezo}$, A accurately represents Δ_u, and the coordinate systems of the measured sample and the laboratory are the same, the lock-in amplitude is given by

$$R = \alpha \cdot d_{ij} \cdot V_{ac}. \tag{7}$$

Determination of α is detailed in Sect. 2.2 below. Typically, the effective d_{33} coefficient in the laboratory coordinate system is measured via VPFM, while LPFM measures the d_{34} and d_{35} elements. Rotating the coordinate system of the sample provides a simple way to access other elements. In practice, several different tensor elements can contribute to the total measured piezoresponse, due in part to imperfect alignment of the coordinate systems but also to the highly inhomogeneous electric field generated by the AFM tip, including nonzero in-plane components, and local symmetry breaks inside the sample.[64,65]

2.2 Calibration

Quantitative determination of the vertical and lateral deformations in PFM is an ongoing challenge due to the inherent complexity of the contact electromechanics of piezoelectric materials with an AFM tip.[66] Ultimately, these deformations can be converted to a measure of the relevant local piezoelectric coefficients, as described in Sect. 2.3.4. In this Section, we review the calibration procedures to convert the piezoresponse amplitude to a measure of the local deformations of the sample surface in response to the applied voltage.

2.2.1 Vertical PFM

The calibration parameter, α, depends on the inverse optical lever sensitivity (invOLS), and the LIA gain, G, as:

$$\alpha = \frac{G}{\text{invOLS}}. \tag{8}$$

Importantly, the definiton of the applied and measured signals is to be kept consistent between the AFM and the LIA: for instance, if the PSD output is measured as peak values and the LIA measures root-mean-square (rms) values, then Eq. (8) contains an additional factor of $1/\sqrt{2}$. For VPFM, the

deflection invOLS is typically measured from the constant compliance region of a contact mode force curve.[67] In this method, an infinite contact stiffness is assumed, and a hard substrate such as glass is used to ensure there is no deformation of the material underneath the tip. An alternative method is to calculate the invOLS using the Higgins method,[68] which has the advantage of not requiring an invasive measurement. The Higgins method is, however, only suitable if the cantilever spring constant can be accurately determined.

Another widely used calibration method consists of measuring a sample having a known piezoelectric coefficient and scaling the LIA output accordingly. In particular, commercially available x-cut quartz has a small but accurately known d_{11} piezoelectric coefficient of 2.3 pm/V,[17] which can be verified using a different distance-sensitive instrument such as a double-beam laser interferometer.[69] Measuring the d_{11} coefficient of x-cut quartz with VPFM corresponds to measuring an effective d_{33} coefficient, as discussed in Sect. 2.3.4. Because the piezoresponse of quartz is small and can therefore be dominated by instrumental offsets at a single applied voltage,[60] a calibration using this method should be performed using ac voltage sweeps (see Sect. 2.3.4). Consideration should also be made to what extent a measurement on a bulk crystal can be applied to samples with reduced dimensions such as thin films and nanostructures.

For both VPFM calibration methods described, it is important to repeat the calibration procedure on a hard surface each time a new cantilever is mounted, since the invOLS depends on both cantilever properties and laser position.

2.2.2 Lateral PFM

Similarly to VPFM, LPFM calibration can be achieved by scaling the lateral signal to the known shear deformation of a standard crystal such as y-cut lithium niobate (d_{15} = 69.2 pm/V).[70,71] Alternatively, the lateral calibration parameter, α_L, can be measured or derived. Several publications reported the use of experimental setups specifically built for LPFM calibration, such as an Al cube[72] or Si slab[73] glued to the side of a piezostack. In the latter study, Peter *et al.* proposed a geometry-based calculation[73] (subsequently corrected by a factor of 2[74]) by which α_L can be derived from α_V as a function of the dimensions of the cantilever (ideally determined using scanning electron microscopy), and verified it experimentally using a piezostack. In 2011, Choi *et al.* proposed an easily accessible method to measure α_L for LPFM as the slope of the lateral signal as a function of increasing scan size.[75]

In contrast to the previous methods, a direct measurement of the torsional invOLS, relating the PSD signal to the torsion angle of the cantilever, can be performed. The key difference is that, while the previously decribed calibration methods need to be performed for each new cantilever setup, measuring the torsional invOLS aims to calibrate the instrument itself. Importantly, for LPFM, the torsional invOLS, measured in units of angle per volt, needs to be converted to the lateral invOLS, which relates the PSD signal to the lateral displacement at the tip apex, measured in units of length per volt. This conversion is purely geometrical and independent of cantilever stiffness. Measuring the torsional invOLS can be achieved by monitoring the lateral signal of the PSD as a function of sample tilt, which can be implemented by mounting a reflective surface such as gold-coated Si on a goniometer. Alternatively, the reflective surface can be kept flat and the AFM head tilted. Regardless of the method used for LPFM calibration, the ratio between the instrument-dependent electronic gains applied to the vertical and lateral signals (not to be confused with LIA gains) can be different; for this reason, it is advisable to measure the transfer functions of the vertical and lateral signals in order to determine the gain ratio as a function of operation frequency.

To this day, LPFM calibration remains less consistently implemented than VPFM calibration, perhaps because of the absence or underutilisation of a recognised standard.

2.3 Practical guide

In this Section, some of the key requirements of quantitative PFM and associated pitfalls are reviewed. As this guide is not meant to be exhaustive, the reader is strongly encouraged to refer to the many excellent guides and reviews previously published.[53–56,58,60,76]

2.3.1 Minimising electrostatic and nonlocal contributions to the piezoresponse amplitude

Quantitative PFM –referring now to the determination of d_{ij} coefficients– requires the A_{el} and A_{nl} contributions to the measured piezoresponse amplitude to be minimised, thus obtaining a signal originating primarily from the electromechanical response of the sample. To this end, good mechanical and electrical contact must be achieved between the tip and the sample surface, e.g., through extensive tip/sample cleaning and sufficient loading force. For completeness, the effects of the tip-sample contact area, tip wear, and cantilever material (conductivity and band alignment with the sample material) should be considered. The use of a cantilever with high stiffness[56] ($k > 1$ N/m) or shielded probes[77] allows the A_{el} and A_{nl} contributions to be reduced. Stiffer cantilevers, however, might be incompatible with soft samples. While they can be minimised, electrostatic contributions can however still be present: in a recent Kelvin probe force microscopy (KPFM) study, Balke *et al.* reported that electrostatic forces can be measured in contact mode with a tip as stiff as 4.5 N/m.[78] This finding highlights the importance of other AFM operation modes such as electric force microscopy (EFM) and KPFM in complement to PFM in order to assess the presence and role of electrostatic contributions, which can be minimised by applying a suitable dc offset (V_{dc} in Eq. (1)).[66,79]

More generally, possible contributions to the measured piezoresponse amplitude include electrostatics,[56] electrochemistry,[24] electrostriction,[80] surface charge states,[81] charge injection,[82–84] and even laser position on the cantilever,[85] which should all be considered. It is worth noting that extraneous contributions to PFM have been associated with the possible inductive coupling between the input and output signals; for this reason, it is generally recommended to use external wiring for the input signal. Rigorous methods to extract the electromechanical contribution from the measured signal include modelling of the electric field generated by the tip,[86] stress distribution solutions based on Green's function,[87] and calculating the displacement field from the stress/strain field using finite element modelling,[88,89] to name a few.

2.3.2 Selecting the operating frequency

In standard PFM, the operation frequency, $f = \omega/2\pi$, of the excitation voltage, V_{ac}, lies typically in the ∼10–100 kHz range. This satisfies two conditions: that f is greater than the bandwidth of the topographical feedback loop of the AFM controller ($f \gg \sim$1 kHz), and that f is small with respect to the contact resonance frequency of the cantilever, f_{CR}, dependent on cantilever properties and the oscillation (flexural or torsional) mode.[60] PFM in the ∼100 kHz–10 MHz frequency range can also be performed, either far from or close to f_{CR}, depending on the AFM instrumentation used.[90] Contact resonance PFM has attracted particular attention as a way to increase the signal-to-noise ratio (SNR), while allowing lower V_{ac} to be applied to achieve SNRs comparable to those obtained off-resonance.[91–93] One advantage of high frequency PFM is the opportunity to scan at higher speeds since the number of periodic voltage-induced tip-sample interactions per pixel is increased. Nath *et al.* have furthermore reported an increase by a factor of 100 with respect to standard scan rates by imaging smooth samples without active topographical feedback.[94] In VPFM, the piezoresponse amplitude is expected to be independent of frequency below f_{CR}; in contrast, the piezoresponse amplitude can decrease with increasing frequency below f_{CR} in LPFM due to the onset of sliding friction[95,96] or from an instrument-dependent frequency roll-off of the lateral signal.

With the application of V_{ac} at a single frequency close to f_{CR}, there exists however a significant crosstalk between the piezoresponse signal and the surface topography; in particular, f_{CR} can vary if the surface is rough, leading to variations in the piezoresponse amplitude, and to erroneous phase data if f_{CR} crosses from below to above the operation frequency or vice-versa. Moreover, single-frequency PFM close to resonance cannot easily be made quantitative, since the piezoresponse amplitude needs to be scaled by the resonance enhancement, which can vary while scanning. These challenges have been addressed with the development of band excitation (BE) and dual ac resonance tracking (DART) modes. In DART PFM, two excitation signals at frequencies $f_{1,2} = f_{CR} \pm \Delta$ are applied, where Δ is of the order of half the width of the resonance peak, and a feedback loop maintains both amplitudes at the same level, thus tracking f_{CR}.[97] In BE PFM, the sample is excited and the response detected

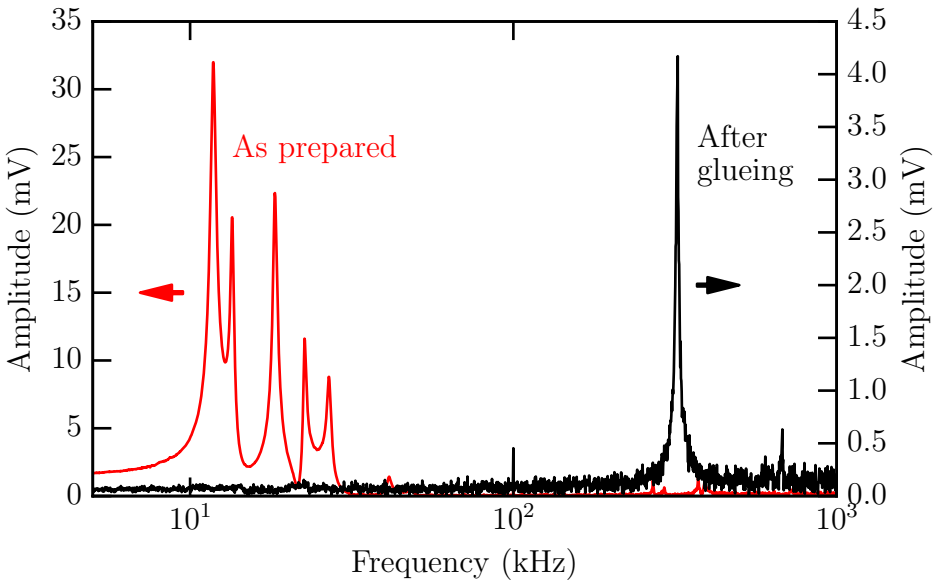

Figure 2: PFM sweeps as a function of excitation frequency measured on a thymine crystal grown from solution, first when just placed on a conductive substrate, and then after having been glued with silver paint.

at multiple frequencies within a defined band typically centered around f_{CR}.[98] Assuming that the electromechanical and elastic responses can be decoupled, DART and BE modes both allow for quantitative PFM provided the piezoresponse amplitude is scaled by the resonance enhancement factor. It was recently demonstrated that the SNR in single frequency close to resonance depends explicitly on the detection system noise and can be effectively lower than predicted by SHO theory;[99] in the same study, the SNR in BE was also found to be reduced by the number of bins used in fitting of the resonance curve. Multifrequency PFM modes allow fundamental parameters of the tip-surface interaction to be quantified: in a mass-spring simple harmonic oscillator model, the resonance frequency and the quality factor ($Q = f_{CR}/\Delta f$, where Δf is the peak width) provide a measure of the conservative and dissipative tip-surface interactions, respectively; the other two independent parameters, the amplitude and the phase, depend on the driving force. Using this opportunity, two DART techniques have emerged that allow nanoscale mapping of the viscoelastic properties of the sample, atomic force acoustic microscopy[100] and ultrasonic atomic force microscopy,[101] which provide a way to decouple elastic and electromechanical properties. Recently, the ability to measure on torsional resonance in BE mode for LPFM has been demonstrated in a liquid environment.[102]

In practice, when performing standard PFM, it is desirable to measure the piezoresponse amplitude as a function of frequency (i.e. to perform a frequency sweep) prior to the experiment in order to choose an appropriate frequency in a flat linear region. This protocol also allows frequency-dependent offsets to be measured.[60] In addition, there can exist additional peaks in the frequency response that arise from the sample mounting or LC resonances in the electronics. This is highlighted in Fig. 2 (a), where frequency sweeps conducted on a centrosymmetric (nonpiezoelectric) thymine crystal are shown. This sample was grown from solution in a beaker and placed on a glass substrate coated with conductive indium tin oxide after drying. It can be seen that a sweep performed on this setup shows several peaks in the ∼10–40 kHz frequency range. In contrast, a sweep performed on the same crystal after glueing it with silver paint only shows a contact resonance peak at $f_{CR} \sim 320$ kHz. Displacements associated with poor sample-substrate contact can lead to a linear response as a function of V_{ac} (observed for this crystal) expected from a piezoelectric material, highlighting the importance of a well defined mechanical contact between the sample and the substrate.

2.3.3 Associating VPFM and LPFM with out-of-plane and in-plane components of the piezoresponse

As discussed in Sect. 2.1, an out-of-plane piezoresponse causes flexural deflection of the cantilever, while an in-plane piezoresponse can cause flexural buckling and lateral twisting. For this reason, a VPFM signal can be measured in the absence of an actual out-of-plane piezoresponse.[96,103] However, the effects of the out-of-plane piezoresponse on VPFM are independent of the orientation of the cantilever, contrary to buckling and twisting. Thus, buckling contributions can be distinguished from deflection contributions by rotating the sample with respect to the cantilever: e.g., if the sample is rotated by 180° horizontally, buckling contributions originating from an in-plane piezoresponse should yield an inverted phase contrast, while no change would be expected from the out-of-plane piezoresponse signal. Since LPFM is only sensitive to the components on the in-plane piezoresponse that are perpendicular to the cantilever axis, at least two different angles are required to measure the orientation of the in-plane piezoresponse. In particular, the LPFM amplitude can be close to zero if the cantilever is aligned parallel to the piezoresponse orientation. The denomination 'piezoresponse orientation' here refers to the axis of mechanical deformation under the applied electric field as given by the piezoelectric tensor of the material in the geometry of the sample; in the specific case of ferroelectric materials, discussed in Sect. 3, this is associated with the orientation of the polarisation.

Different types of cantilever can be better suited for VPFM or LPFM, depending on their geometry and stiffness. In particular, a theoretical analysis by Sader showed that, contrary to the common perception, V-shaped cantilevers should be more sensitive to the effects of lateral forces than rectangular cantilvers.[104]

2.3.4 Measuring d_{ij} coefficients

In general, quantitative PFM is limited by the presence of offsets (mostly of electronic origin) in the piezoresponse amplitude, which yield an additive term to Eq. (7). For this reason, piezoelectric coefficients should not be determined from single-voltage measurements. Rather, the piezoresponse amplitude should be recorded as a function of V_{ac}: the slope of the resulting graph yields a value independent of offsets, $\alpha \cdot d_{ij}$, measured in volt. The piezoelectric coefficient can be extracted from this slope value if the calibration parameter, α, is known, as described in Sect. 2.2. As mentioned in Sect. 2.3.2, a good mechanical and electrical contact between the tip and the sample is particularly important in order for these measurements to be quantitative.

As discussed in Sect. 2.1, the deformations of a piezoelectric material under an applied voltage are characterised by a third-rank tensor, d_{ijk}, and are therefore highly directionally dependent.[61] Thus, in a PFM experiment, if the sample being investigated has an arbitrary orientation, the measured piezoresponse may actually comprise contributions from several piezoelectric coefficients.[53,105] This poses a challenge for measuring real (not effective) piezoelectric coefficients. If the symmetry of the material is known in addition to its orientation with respect to the applied electric field (laboratory coordinates), then elements of the piezoelectric tensor in the crystal coordinate system can be determined from the elements measured in the laboratory coordinates.

2.4 Spectroscopic modes

Recent advances in PFM techniques include the ability to probe dynamic charge phenomena with high temporal and spatial resolution. This ability is particularly suited to ferroelectric materials, whose spontaneous polarisation can be switched under an applied electric field, and which form the focus of Sect. 3. In 2006, Jesse *et al.* reported such a technique, called switching spectroscopy PFM (SS-PFM), where successive pulses of applied voltage of increasing amplitude are applied and the piezoresponse can be measured both in-field or in between switching pulses.[106] As further discussed in Sect. 3, this method allows the polarisation switching events to be quantitatively mapped. Another approach is first-order reversal curve (FORC) mapping, which provide insight into the relative proportions of the reversible and irreversible components of the sample underneath the tip.[107] In these approaches, the complexity of the data and therefore the gathered information are significantly larger than in standard PFM.

3 PFM of inorganic ferroelectrics

3.1 Background

While piezoelectricity lies at the heart of PFM, both initial and recent developments of this technique were made in the context of ferroelectric materials.[108] In addition to piezoelectric and pyrolectric properties allowed by a noncentrosymmetric crystal structure, ferroelectrics are furthermore characterised by a spontaneous electrical polarisation that can be reversibly switched between two or more nominally energetically-equivalent ground states under an external electric field. Regions within ferroelectric samples of identical polarisation state are called ferroelectric domains and may extend to just a few unit cells in size, separated by unit-cell-thin boundaries called domain walls. Ferroelectric domains form naturally in ceramics, single crystals, and thin films alike in order to minimise the total free energy depending on the depolarizing field, domain walls, ferroelastic contributions, and external conditions,[109,110] exhibiting a variety of patterns such as stripes,[111] quadrants,[112] and vortex structures.[113] The development of nanoscale observation techniques such as PFM have allowed the nucleation, propagation, and stability of individual domains to be studied and tailored towards their integration into increasingly miniaturised devices. This concerns both artificial domains written with the AFM tip, the most well-known application being FeRAMs,[39,40] and intrinsic domains. The presence of domains in ferroelectric samples has been demonstrated to affect macroscopic properties such as the dielectric susceptibility[5] and piezoelectric response.[6,7] Therefore, understanding and controlling domain structures is key to tailoring and optimising the electronic properties of ferroelectric materials. Recently, Lichtensteiger *et al.* have demonstrated using PFM that the insertion of a dielectric spacer layer between a ferroelectric thin film and the bottom electrode led to an increase of the depolarizing field, allowing a polydomain configuration to be tailored in samples presenting a uniform polarisation. They furthermore observed that the domain size and pattern in the presence of a spacer layer could be tuned as function of the ferroelectric film thickness.[114] Many studies in the past few years have specifically focused on the physics of domain walls, revealing them to harbour properties absent from the bulk material, similarly to other interfaces such as bicrystal grain boundaries[115] or heterostructures.[116,117] Typical examples include electrical conduction[118] and photovoltaicity,[119,120] which have led to the emergence of domain wall nanoelectronics as a topic of its own.[121,122] Another domain-wall-specific property, the nonzero lateral piezoresponse of 180° domain walls in a tetragonal ferroelectric,[88] was revealed by PFM. Thus, the applications of PFM to investigate ferroelectric materials span an important range of physical behaviours, including notably polarisation switching characteristics, configurations and stability of static domain, domain dynamics, and domain wall properties.

3.2 Ferroelectric nanoscale imaging

Conventional PFM has been used extensively to study the static properties of ferroelectric domains, providing a way to image naturally present domain patterns or AFM-written domains with nanometric lateral resolution. With the presence of a stable electrical polarisation within the material, the phase of the piezoresponse gives information on the orientation of the polarisation. VPFM is associated with a polarisation perpendicular to the sample plane, and as such an immediate choice in samples presenting an out-of-plane polarisation component, in particular when the polarisation is purely out-of-plane such as in tetragonal ferroelectric thin films. A map of VPFM phase showing ferroelectric domains in tetragonal $Pb(Zr_{0.2}Ti_{0.8})O_3$(PZT) as a two-colour contrast of 180° is shown in Fig. 3 (a). Concurrently, the PFM amplitude (Fig. 3 (b)) is proportional to the d_{33} coefficient of *c*-axis oriented epitaxial PZT and shows no contrast between domains, with a drop observed only at domain walls due to the cancelling contributions of opposite domains at either side of the tip. Where present, the in-plane component of the ferroelectric polarisation is observed via LPFM.

In practice, a variation in amplitude levels between domains can be observed, often accompanied by a phase difference less than 180°. These artefacts are sometimes attributed to electrostatic effects originating from screening charges and surface adsorbates. However, the recent study by Labuda and Proksch[63] on the effects of laser spot position on the back of the cantilever suggests that cantilever dynamics also contribute to these effects.

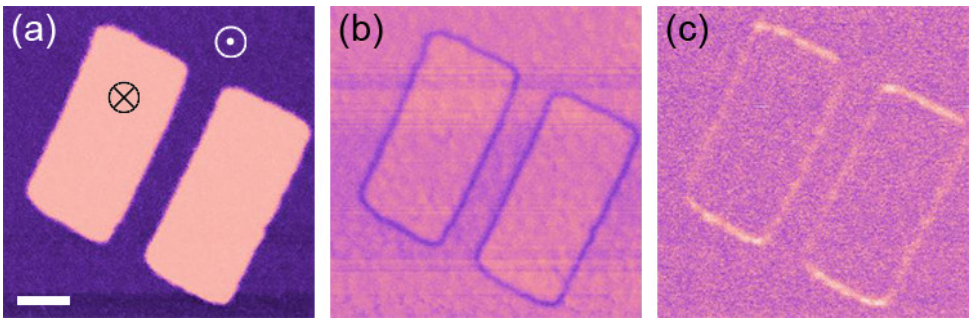

Figure 3: PFM imaging of two rectangular domains in a tetragonal PZT thin film with strictly out-of-plane polarisation. (a) VPFM phase map, showing 180° contrast between positively poled 'down' (⊗) domains and as-grown background 'up' (⊙) polarisation. Scale bar is 0.5 µm. (b) VPFM amplitude map, showing a signal drop at domain walls. (c) LPFM amplitude map, showing a nonzero contribution at domain walls arising from nonzero effective dielectric tensor elements due to local symmetry lowering. Adapted with permission from Guyonnet *et al.*,[127] copyright 2009, American Institute of Physics.

As discussed in 2.3.3, LPFM is dependent on the orientation of the cantilever, and several measurements taken at different angles are sometimes needed in order to achieve three-dimensional reconstruction of the polarisation orientation.[123] In multiferroic $BiFeO_3$ (BFO) samples presenting 8 variants of ferroelectric in-plane polarisation, Park *et al.* have shown using angle-resolved PFM that by rotating a sample in 30° increments, more unambiguous information on in-plane polarisations can be obtained.[124] Furthermore, buckling contributions to the VPFM signal as well as topographical cross-talk strongly encourage the practice of angle-resolved PFM to discriminate true contributions of the ferroelectric polarisation.[60,125] An LPFM signal that is piezoelectric in nature can however be observed in samples devoid of in-plane polarisation, at the position of 180° domain walls, as shown in Fig. 3. Originally attributed to surface deformations[88] and subsequently to electrostatic effects,[126] this LPFM signal was subsequently shown to be incompatible with a surface deformation scenario and independent of surface charging.[127,128] More recently, resolution function theoretical modelling showed that the local breakdown of symmetry at domain walls leads to additional nonzero elements of the effective piezoelectric tensor, thus confirming the piezoelectric nature of this phenomenon.[64,89]

Beyond ferroelectrics, PFM has played a central role in multiferroic materials, which present two or more ferroic orders.[129] In multiferroics presenting both ferroelectric and magnetic ordering, the presence of a magnetoelectric coupling has sparked significant interest for novel applications such as multistate memories.[130] Amongst single-phase multiferroics, BFO remains the most actively researched materials, combining ferroelectric and antiferromagnetic orderings. Using PFM, Catalan *et al.* reported that ferroelectric domains in BFO thin films are not well described by the Landau-Lifschitz-Kittel scaling law satisfied by purely ferroelectric films, exhibiting a scaling behaviour closer to that of magnetic materials.[131] PFM has also been central in the studies on ferroelectric domain wall conduction[118,132] and photovoltaicity[119,120] as a way to distinguish between the three types of domain walls present in BFO. The ferroelectric polarisation switching characteristics of BFO has been the focus of numerous studies, as discussed in Sect. 3.3.[133–136] While the phase diagram of BFO has been under investigation for several decades[137] and the search for other single-phase multiferroics has been intense, few new single-phase multiferroics have been identified until recently.[138–140] Most of these materials, however, are not multiferroic at room temperature, with few exceptions including $LuFeO_3$[141] and $Bi_6Ti_{2.8}Fe_{1.52}Mn_{0.68}O_{18}$ thin films.[142] Multiferroic heterostructures, in which a ferroelectric and a magnetic phase are coupled through strain, exchange bias, or charge, have been presented as an alternative to single-phase multiferroics.[116,143–147] Recently, Evans *et al.* reported a change in ferroelectric domain patterns after the application of a magnetic field in solid solutions of ferroelectric PZT and antiferromagnetic $PbFe_{0.5}Ta_{0.5}O_3$, showing them to be ferroelectric and ferromagnetic with magnetoelectric coupling at room temperature.[148] Similarly, Trivedi *et al.* mapped out the impact of an applied magnetic field on the polarisation switching processes in $BaTiO_3$–$BaFe_{12}O_{19}$ composites using SS-PFM and and spatially resolved confocal Raman microscopy.[149]

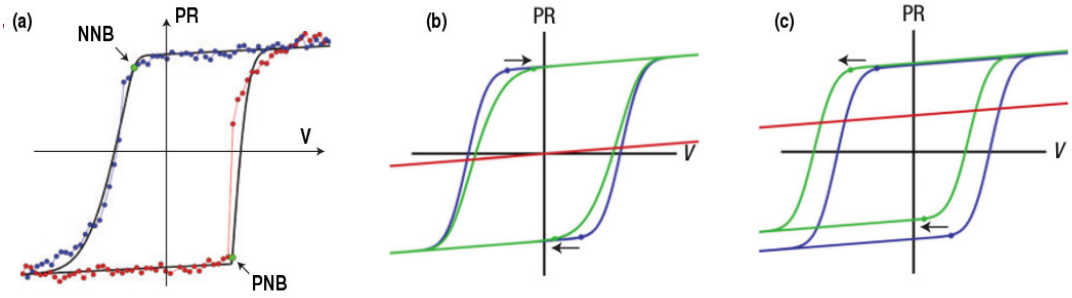

Figure 4: Assessing polarisation switching and disorder universality class by SS-PFM. (a) SS-PFM experimental hysteresis, showing the positive (PNB) and negative (NNB) nucleation biases. (b,c) Effect of random-bond (b) and random-field (c) disorder on hysteresis. The blue curves correspond to the ideal case of a defect-free sample, the green curves to weak disorder, and the red curves to the extreme cases of a nonpolar and a polar non-ferroelectric phase, respectively. Arrows indicate the direction of the measurement. Reprinted with permission from Jesse *et al.*,[150] copyright 2008, Nature Publishing Group.

3.3 Ferroelectric switching with AFM

3.3.1 Quantifying tip-induced switching

Quantitatively understanding how polarisation reversal proceeds in ferroelectrics on a scale spanning just a few unit cells is central to enable miniaturised applications. The nanometric contact area between a conducting AFM tip and the surface of the ferroelectric sample allows the application of highly localised electric fields. Thus, polarisation switching can be initiated from a single domain nucleated directly below the tip. Using this approach, the switching dynamics may be locally accessed and mapped out over regions extending to tens of square micrometres. Conventionally, this is done by ramping the bias voltage of the tip while recording the PFM amplitude, leading to a characteristic hysteresis loop reminiscent of the macroscopic polarisation vs. applied electric field hysteresis. However, while macroscopic hysteresis results from the nucleation, growth, and interaction of several domains, PFM allows the switiching characteristics of a single domain to be accessed. In this respect, SS-PFM allows real-space mapping of quantitative parameters of switching dynamics such as hysteresis width or imprint.[106] In particular, the universality class of the disorder associated with quenched defects (random-bond or random-field) can be mapped out,[150] as illustrated in Fig. 4. More recently, band excitation PFM was used to tie Rayleigh behaviour present in the subcritical field regime to long-range collective domain wall dynamics in ferroelectric polycrystalline capacitors.[151] Following the need to assess small field behaviour and the impact of disorder on switching dynamics, Ovchinnikov *et al.* applied the first-order reversal curve method to PFM, allowing the Preisach density to be spatially mapped.[152] Using this technique, the individual polarisation switching behaviour in $BiFeO_3$ nanocapacitors was shown to depend on pre-existing domain patterns.[107] In a comparative study on epitaxial $(0.3)Pb(Ni_{0.33}Nb_{0.67})O_3$-$(0.7)Pb(Zr_xTi_{1-x})O_3$ thin films, Griggio *et al.* showed that higher domain wall mobility led to greater dielectric and piezoelectric nonlinearities for samples in the rhombohedral phase as opposed to those grown in the tetragonal phase or close to the morphotropic phase boundary.[153] All of these recent studies highlight the key role of disorder and long-range correlations on hysteretic behaviour in ferroelectrics and the ability of advanced PFM techniques to resolve this behaviour despite the local nature of the measurement.

3.3.2 Deterministic switching

Within the emerging interest for multi-level memory storage devices, ferroelectrics presenting more than two possible polarisation orientations have been suggested to allow significantly increased density with respect to traditional FeRAMs. One such material is multiferroic BFO in the rhombohedral-like monoclinic phase, in which the ferroelectric polarisation has 8 different possible orientations. In 2009, Balke *et al.* demonstrated that deterministic polarisation switching can be obtained in BFO

through lateral tip motion, which effectively breaks the rotational symmetry of the applied electric field.[133] Subsequently, Béa *et al.* distinguished the switching behaviour induced by tip motion in samples presenting different intrinsic domain patterns.[134] Vasudevan *et al.* explored possible transition pathways in mixed-phase tetragonal-rhombohedral (T-R) BFO,[135] and Chen *et al.* achieved deterministic control of T-R boundaries controlled by the tip trajectory.[136] More recently, the ability to deterministically rotate the polarisation to an arbitrary mesoscale orientation was demonstrated in multiferroic nanocomposites, attributed to the existence of sub-50 nm domains and the absence of long-range ordering.[154]

3.3.3 Effects of environment

Due to the nanometric size of the apex of the AFM tip, the applied electric field in conventional PFM is both highly localised and non-uniform. Thus, several analytical[155] and numerical[156,157] models have been devoted to quantify the spatial extension of the field. In practice, the field is strongly dependent on the tip conditions, including shape, radius, and size of the contact area. However, studies performed in ambient conditions have shown domain growth to be significantly dependent on the relative humidity,[81] which can be tied to the formation of an adsorbed water layer on the sample surface and of a water meniscus around the tip. Different explanations have been proposed for the actual mechanism that leads to a change in the electric field: static finite-element simulations studies have suggested that the water meniscus could act as an effective electrode,[156] while similar simulations with an additional time evolution reported a slow lateral propagation of the electric field.[157]

Recent studies addressing both relative humidity and the effects of switching voltage pulse sequence[158] highlight the necessity to incoroporate environmental contributions to field modelling.

3.3.4 Switching through a planar top electrode

While ferroelectric switching experiments using the AFM tip as a top electrode have the characteristics of nucleating a single domain under the tip, the exceptions to this are when the experiment is performed in a liquid environment with sufficient electrical conduction[159] or in a capacitor geometry.[160] In the presence of a large top electrode, the applied electric field is homogeneous throughout the capacitor. In terms of imaging, quantitative PFM is therefore generally more straightforward, unless capacitor bending is present.[161,162] Another advantage is the very small influence of tip quality, as field inhomogeneities rather come from defects in the electrode-sample interface.

While many groups have been able to image domains through the top electrode,[163–165] Kalinin *et al.* have shown that PFM resolution is lower, with the thickness of a ferroelectric domain wall measured by PFM scaling linearly with the thickness of the top electrode.[166] PFM switching experiments using capacitor-geometry samples allow a different approach in which the spatial variations of switching events and properties can be mapped out on a scale ranging from submicron to tens of micrometres, limited only by the top electrode or maximal scan size. Due to the presence of a homogeneous electric field, domains nucleate at specific nucleation sites where either the electric field is enhanced or the ferroelectric potential is lowered. This feature is clearly apparent in the stroboscopic approach developed by Gruverman *et al.*,[167,168] where nucleating pulses of increasing duration are applied in alternance with setting pulses that revert the polarisation to a uniform state. Although nucleation from a uniformly polarised state is partially stochastic in nature, such studies have allowed the switching behaviour to be characterised as a function of capacitor size on a sub-100 ns time scale. In order to circumvent changes due to stochastic nucleation, a so-called cumulative switching approach[168] was then adopted, in which a succession of n switching pulses is assumed to lead to a comparable configuration as a single pulse of identical length.[169] The group of Noh has shown that this approach is critical to probe the frequency-dependent dynamics of domain walls in ferroelectric capacitors.[170] Blaser *et al.* recently could only verify this assumption for pulses above 10 ms for tip-nucleated domains in PZT thin films.[158]

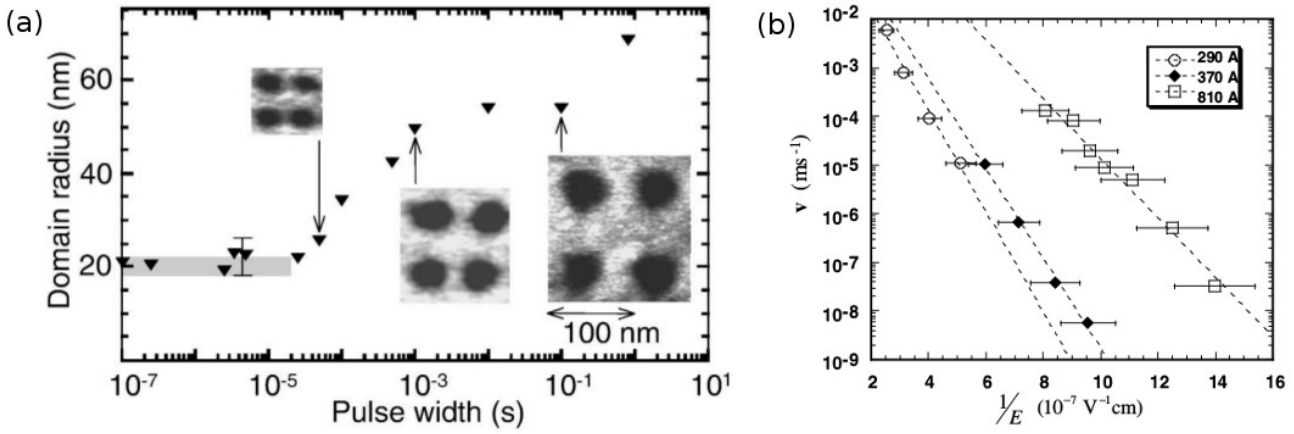

Figure 5: Tip-written ferroelectric nanodomains in PZT thin films. (a) Logarithmic dependence of the domain radii as a function of writing voltage pulse length. Domain size saturation is observed for pulse lengths shorter than ∼20 µs. (b) Domain wall velocity as a function of inverse applied electric field (calculated from the applied voltage) for samples with different thicknesses. In this study, the creep exponent was measured to be close to 1. Reprinted with permission from Tybell *et al.*,[171] copyright 2002, American Institute of Physics.

3.4 Ferroelectric domain dynamics

3.4.1 Measuring domain wall velocity by standard PFM

PFM is a powerful method for investigating the lateral growth of ferroelectric domains, providing microscopic details on domain wall propagation and pinning by defects. Understanding domain dynamics is essential in applications based on controlled domain engineering, all the more so as it has been shown to critically depend on both intrinsic (defect concentration of the sample) and extrinsinc (environment) parameters. Domain wall velocity has been a particularly researched quantity in studies using either conventional PFM[171] or spectroscopic PFM in microscale[169] and nanoscale[172] capacitors. A delicate issue is the actual definition of the velocity, in particular for tip-written domains. In the simplest approach, the growth dynamics can be related to the size of single domains written with different bias voltage pulse amplitudes and lengths. Here, the growth velocity, v, between two domains written with successive pulse lengths t_i and t_{i+1} can be defined as $v = (r_{i+1} - r_i)/(t_{i+1} - t_i)$, where r_i and r_{i+1} are the associated domain radii. In this approach, domains are considered stable and unaffected by PFM, and the cumulative switching hypothesis is implicitly assumed. Moreover, there is a minimal domain size set by energy considerations and tip size. Depending on the relative humidity, the water meniscus formed around the tip apex also plays a role, effectively augmenting the size of the top electrode.[158] After the external field is switched off, domains undergo a stabilisation to accommodate for nearby defects and line tension, leading to shrinking and possibly backswitching for critically small sizes.[173,174] Finally, the presence of imprint (preference for one polarisation orientation due to the presence of an in-built bias) strongly affects the growth behaviour, leading to different critical sizes and growth velocities between differently oriented domains. In such studies, the radii of nanodomains measured in epitaxial thin films and single crystals have been shown to typically vary linearly with the applied voltage amplitude and logarithmically with the pulse width.[175,176] An example of this behaviour is shown in Fig. 5 (a), where tip-written nanodomains follow a logarithmic growth above a critical ∼ 20 µs writing time. In combination with field modelling, the domain wall velocity has been reported to follow the empirical relationship known as Merz's law for small applied field: $v \propto \exp(E_a/E)$, where E is the applied field and E_a is the activation field of the wall motion.[169,171]

3.4.2 Disordered elastic systems model for domain wall motion

Theoretical models addressing the dynamics of ferroelectric domain walls can generally be divided into two complementary approaches. The first approach proceeds from a Ginzburg-Landau-Devonshire

formalism, where two or more phases are set to compete at their common boundary.[177–179] Phase-field models have in particular allowed domain patterns, nucleation, and growth to be described.[180] The second approach focuses exclusively on the boundary, which is treated as an independent system, and the underlying microscopic details are ignored.[181] In this case, the interface formed by the domain wall can thus be described by the very general model of a fluctuating elastic interface in a disordered medium, and complex, glass-like physics emerges solely from the competition between elasticity and disorder. The resulting disordered elastic systems (DES) framework is also applicable to a wide range of seemingly different systems, including fracture lines,[182] imbibition[183] and flame[184] fronts, the edge of bacterial colonies,[185] and cell membranes.[186] The most notable advantage of DES theory is that it directly relates the static and dynamic behaviours of interfaces to specific fundamental quantities such as the universality class of the disorder. For a driven interface such as a domain wall subjected to an external field, there exist two main dynamic regimes corresponding to subcritical and above-critical fields, respectively called creep and flow, and separated by a depinning transition. For small applied fields, the creep regime is highly nonlinear: $v \sim \exp\left[-\beta U_c \left(E_c/E\right)^{\mu}\right]$, where E_c is the critical field for domain wall depinning, U_c is a characteristic energy barrier height, and the creep exponent, μ, depends on the disorder and dimensionality of the system. Merz's law corresponds to the creep regime with $\mu = 1$, suggesting that the latter might be a more general description; however, accurately measuring the μ by PFM can prove difficult due to statistical variations owing to the sample properties[187] and the effect of environment.[188] In the 2002 study by Tybell *et al.* on PZT thin epitaxial films, the growth velocity of the domains shown in Fig. 5 (a) was found to be fitted to the creep law with $\mu = 1$. More recent similar studies[187,189] reported values $\mu \approx 0.5$ compatible with the scenario of two-dimensional domain walls in presence of long-range dipolar forces, also observed in the static roughness scaling of the domain walls. Interestingly, another similar study by Pertsev *et al.* on PZT ceramics[190] has reported a value of $\mu \approx 0.25$, consistent one-dimensional wall behaviour. Notably, Pertsev *et al.* previously observed a very different value of $\mu = 0.5$ in $BaTiO_3$ epitaxial thin films.[191] In ferroelectric capacitors, both creep and flow regimes can be accessed, as shown by cumulative switching experiments where the coercive field was revealed to obey a scaling law as a function of frequency with two distinctive regimes.[170]

3.4.3 Ferroelectric capacitors

Several analytical models have been developed to describe the domain nucleation and growth kinetics of ferroelectric capacitors. In micrometre scale capacitors, the model developed by Kolmogorov[192] and Avrami,[193] subsequently extended to ferroelectric materials by Ishibashi[194] (KAI model), has been verified on both single crystals[195] and thin films.[196] The KAI model assumes randomly distributed nucleation sites (corresponding to weak collective pinning in DES theory) and unrestricted domain wall motion in a infinite medium. For this reason, limitations of this model have been associated with either material inhomogeneities or reduced dimensions. For example, Tagantsev *et al.* have proposed a nucleation-limited-switching model to explain the broad switching time distribution in polycrystalline capacitors, attributed to the presence of regions with independent switching kinetics.[197] On the other hand, the KAI model does not describe switching in nanoscale epitaxial capacitors, where the nucleation sites and event are no longer described by classical statistics. For this reason, a finite-size term to the KAI model was first added by Shur *et al.*[198] More recently, non-KAI switching was observed by Kim *et al.* in nanoscale epitaxial capacitors with only one nucleation site.[172] This behaviour was adequately described by a simple model based on nucleation and subsequent domain growth, thus bearing resemblance to tip-written domain growth kinetics.

3.5 Outlook

Since its early development, PFM has been applied to the study of ferroelectric materials, revealing a considerable range of applications from quantifying polarisation switching properties to probing and controlling domain stability and growth. PFM also allows the probing of complex phenomena such as the mesoscopic polarisation ordering in ferroelectric relaxors. In particular, Kholkin *et al.* used a combination of PFM, switching, and spectroscopic experiments to demonstrate the existence two

effective order parameters associated with the static and dynamic parts of the polarisation.[199] The crucial effects of environment on domain size and configuration, reported as early as 2006 by Dahan *et al.*,[81] remain under active investigation, showing intrication with other parameters including applied voltages, pulse sequence, and defect density. However, radically different behaviours observed between PZT[158] and $LiNbO_3$[200] samples suggests that electrochemical contributions play a key role and need to be considered both in theoretical modelling and experimentally through complementary approaches, including ESM. Other AFM techniques have already been shown to be crucial to complement PFM studies of ferroelectric materials, with prominent examples including EFM and KPFM to assess the role of screening charges[66,79] and conductive tip AFM revealing reversible and irreversible switching events at domains walls during PFM.[201] The already important scope offered by AFM can moreover be broadened to include electron microscopy: transmission electron microscopy, in particular, has allowed the near-Ising, structurally complex nature of ferroelectric domains walls[173] and domain switching[202] to be directly observed. Electron backscattered diffraction has been shown to allow quantitative determination of the piezoelectric tensor in polycrystalline and nanostructured samples by resolving the crystalline orientation at the nanoscale.[203,204] Other promising approaches include full field (as opposed to scanning) electron microscopy techniques:[205] photoemission electron microscopy,[206] low energy electron microscopy and mirror electron microscopy allow micrometre scale real-time imaging of ferroelectric domains with a lateral resolution of just a few tens of nanometres, suggesting interesting uses to study switching and domain dynamics. Controlled polarisation switching has even been demonstrated with MEM.[207] Finally, very recent studies have shown that domain walls can controllably be injected at desired positions,[208] with the abilty to reproducibly and reversibly engineer multiple walls.[209] Thus, the emerging role of ferroelectric domain walls as nanoelectronic components in the past few years suggests that PFM will play a key role towards domain-wall-based nanocircuit development.

4 PFM of piezoelectric semiconductors

4.1 Background

Although PFM has primarily been used to characterise ferroelectric materials, PFM has long been applied to the local piezoelectric characterisation of a variety of materials, including piezoelectric semiconductors.[210] Christman *et al.* reported local d_{33} measurements of ZnO films (2–13 pm/V) and x-cut quartz (1.4–1.9 pm/V) as early as 1998.[211] In fact, few previous reports discussed quantification of the measured piezoelectric deformations.[34,212] The motivation for using PFM to characterise piezoelectric semiconductors has been driven largely by the potential applications of such materials, including for polarity-dependent electronic and optoelectronic devices,[213,214] energy harvesting,[215,216] etc., but also as a characterisation tool to determine the polarity of the films and nanostructures grown and their piezoelectric coefficients. Interestingly, early direct macroscopic measurements of the effective transverse piezoelectric coefficient of AlN films[217] has parallels to recent local AFM measurements of bending-induced potentials of piezoelectric semiconductor nanowires.[218] Some researchers have attempted to combine ferroelectrics with piezoelectric semiconductors,[219] demonstrating ferroelectric gate-control of the transport properties of the two-dimensional electron gas at the AlGaN/GaN interface.[220] Notably, the two-dimensional electron gas at the $LaAlO_3/SrTiO_3$ interface[221] may be controlled locally by application of dc bias with a conducting PFM tip as discussed in Sect. 6.[222] Here, the discussion centers on the use of PFM to investigate the piezoelectric semiconductors, GaN, AlN, and ZnO.

4.2 PFM of GaN and AIN

PFM was first demonstrated on III-nitrides in 2002 on a lateral polarity GaN heterostructure comprising adjacent Ga- and N-polar surface regions grown by molecular beam epitaxy on patterned buffer layers.[223] Measurements of AlN films grown by sputtering,[224–226] metalorganic vapor phase epitaxy,[227] and molecular beam epitaxy,[228] bulk AlN crystals[229] and polycrystalline AlN samples,[230,231] quickly followed.

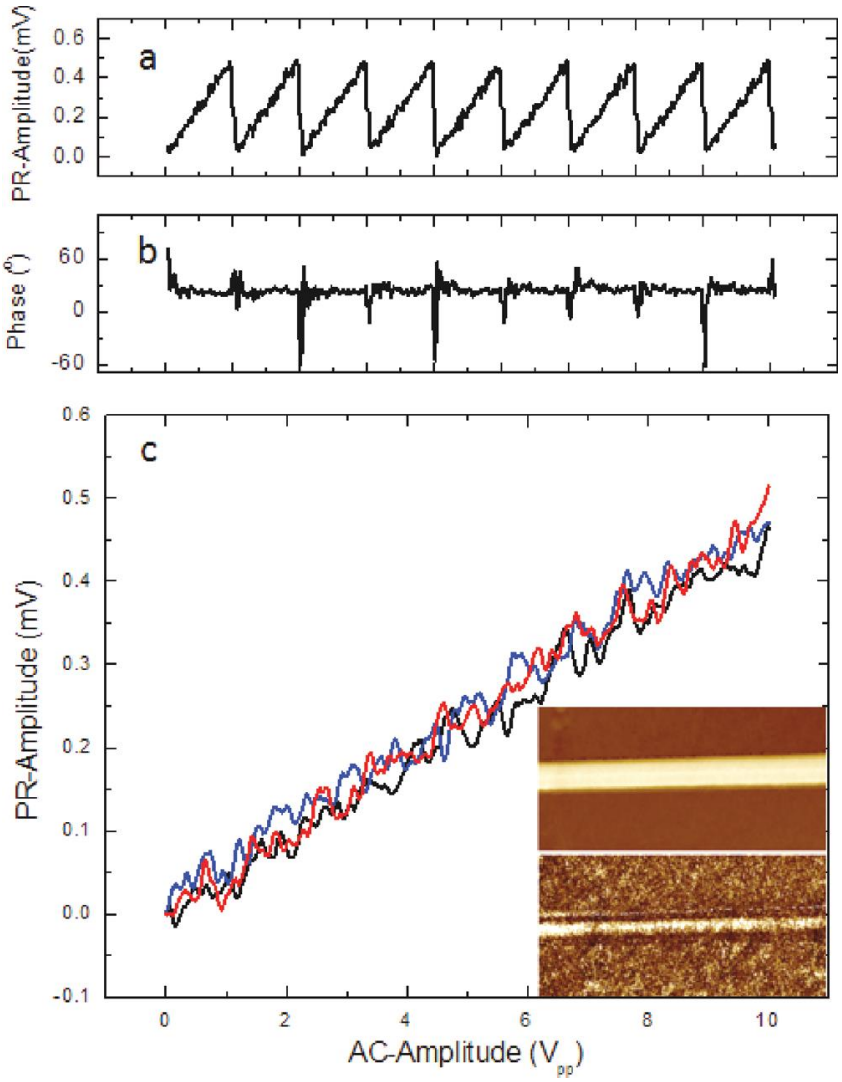

Figure 6: LPFM measurements of the local shear piezoresponse signal in the axial direction of a 170 nm high GaN nanowire. (a) Nine sequential measurements of the V_{ac}-dependence (0 to 10 V with 20 s period) of the LPFM signal, highlighting the reproducibility of measurements performed in the same location. (b) The corresponding LPFM phase signal, demonstrating the uniformity of the phase response during the application of V_{ac}. (c) Linear V_{ac}-dependence of the local shear piezoresponse amplitude signal recorded at three locations along the nanowire. The topography and LPFM amplitude of a 64 nm high nanowire is shown in the inset (2 µm scan). Reprinted with permission from Minary-Jolandan *et al.*,[232] copyright 2012, American Chemical Society

Notably, Lee *et al.* measured the V_{ac} dependence of the piezoresponse amplitude signal to determine d_{33} (3.8 pm/V),[224] and Tonisch *et al.* directly compared local PFM and macroscopic piezoelectric interferometry measurements of d_{33} for the same film (5.4 versus 5.5 pm/V, respectively).[231] In 2007, Stoica *et al.* reported PFM imaging of molecular beam epitaxy-grown GaN films, showing for the first time conditions where the LPFM signal could be detected and an influence of dc bias on the VPFM signal.[233] Recently, Zukauskaite *et al.* reported an increase in d_{33} in sputtered $Sc_xAl_{1-x}N$ thin film alloys with increasing Sc concentration up to $x = 0.2$, in agreement with theoretical predictions,[234] and Babu *et al.* reported local piezoelectric measurements of sputtered AlN/CoFe bi-layer thin films as a function of externally-applied in-plane magnetic field strength, highlighting the presence of a stress-mediated magnetoelectric coupling.[235] PFM has also been applied to investigate the piezoelectric properties of GaN nanowires (Fig. 6), demonstrating the first LPFM measurement of shear piezoelectricity in III-nitride nanowires, and the measurement of d_{33}, d_{13}, and d_{15} piezoelectric coefficients (12.8, -8.2, and -10.2 pm/V, respectively).[232,236]

4.3 PFM of ZnO

Following the work of Christman *et al.* on sputtered ZnO thin films, Zhao *et al.* used PFM to measure d_{33} of ZnO nanobelts in 2004, comparing the results to x-cut quartz and bulk ZnO (Fig. 7).[237] The piezoelectric properties of the nanobelt were reported to be frequency-dependent below the contract resonance of the AFM cantilever, decreasing in signal with increasing frequency. Another study reported an increase in piezoresponse with increasing frequency for ZnO nanobelts.[238] PFM imaging and local d_{33} measurements have also been measured for large-order arrays[239] and individual nanorods of ZnO.[240] In 2008, Scrymgeour and Hsu reported combined PFM and conducting-AFM measurements of ZnO nanorods (Fig. 8), finding that d_{33} was higher for more resistive nanorods.[241] Previously, based on nanorod measurements ($d_{33} = 4.41 \pm 1.73$ pm/V), Scrymgeour *et al.* reported that PFM measurements were not correlated with height and exhibited weak linear correlation with diameter.[240] PFM has also been used to investigate the piezoelectric properties of sputtered,[242,243] and sol-gel[244] prepared thin films. Schuler *et al.* reported high-resolution inversion domain boundaries on the order of 1.5 nm in sputtered ZnO thin films.[242] Patterned buffer layers have been used to prepare one- and two-dimensional ZnO lateral polarity heterostructures, the latter of which have been imaged using PFM.[245,246] Local PFM measurements recorded as a function of dc bias showed differences in the piezoresponse for Zn- and O-polar regions.[245] Vector PFM was used in textured ZnO thin films by Bdikin *et al.* to measure the piezoelectric coefficients and map out the unipolarity of the films.[247] Transition metal-doped ZnO films and nanostructures have been widely studied by PFM, often revealing a ferroelectric-like character of the local PFM hysteresis loop measurements,[248–251] or evidence of local dc bias-induced switching.[252]

4.4 Outlook

PFM has long been used to characterise piezoelectricity in semiconductors and will likely continue to find application considering the recent developments in piezoelectric nanogenerators and energy harvesting. Piezoelectric semiconductors further provide a contrasting platform for comparison to ferroelectric materials, allowing the role of defects and charge screening to be investigated. Morozovska *et al.* has reported on the behaviour of ferroelectric semiconductors probed by PFM spectroscopy,[253] however, theoretical considerations of frequency- and size-dependent piezoelectricity (and piezochemistry[254] and flexoelectricity[255]) of semiconductors are needed. There remains scope to combine scanning probe microscopy approaches such as conducting-AFM, EFM, KPFM, and advanced spectroscopic PFM modes,[256,257] to more completely characterise the materials studied. Furthermore, the second harmonic of the PFM signal could be used to investigate electrostriction in, e.g., GaN.[258] Given recent advancements in the interpretation of electrochemical strain microscopy data[259] and local surface modifications and reactions by AFM,[260] early data on local electrochemical surface modification of AlGaN/GaN heterostructures[261] should be revisited and these new approaches should be applied to piezoelectric semiconductors.

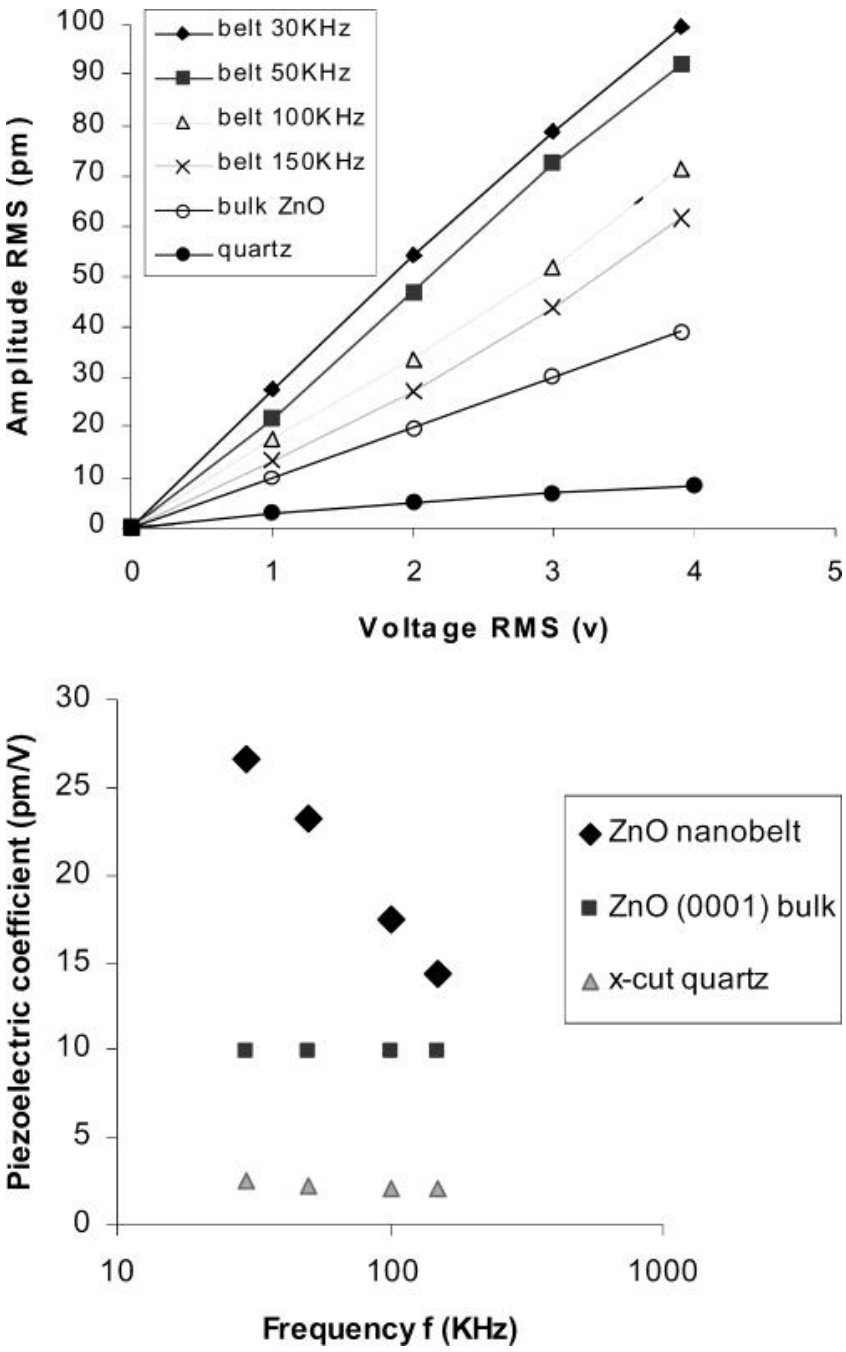

Figure 7: Comparison of the piezoelectric propertiers of a ZnO nanobelt, bulk ZnO, and x-cut quartz. (a) Linear V_{ac}-dependence of the piezoresponse signal, measured at different frequencies for the nanobelt. (b) The calculated piezoelectric coefficient (slope of plots in (a)) for the same samples as a function of frequency. Reprinted with permission from Zhao *et al.*,[237] copyright 2004, American Chemical Society.

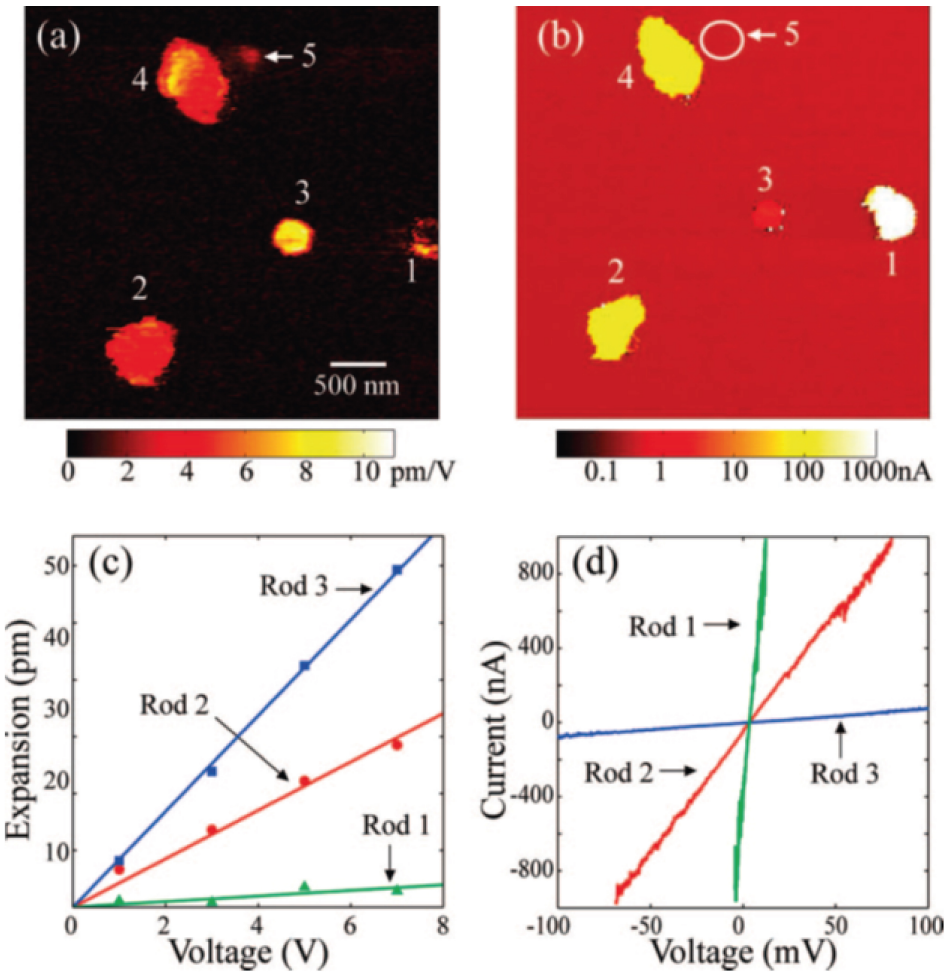

Figure 8: PFM of ZnO nanorods. (a) PFM amplitude image (in pm/V) and (b) conducting-AFM image of the same area recorded with a dc bias of 10 mV. (c) Linear V_{ac}–dependence of the piezoresponse signal measured for three rods, showing the largest response from rod number 3. (d) Current plotted as a function of applied dc bias measured for the same three rods, showing the lowest signal (highest resistivity) for rod number 3. Reprinted with permission from Scrymgeour and Hsu,[241] copyright 2008, American Chemical Society.

5 PFM characterisation of organic and biological systems

5.1 Background

Electromechanical coupling is ubiquitous in organic and biological systems[262] and associated with muscle contraction,[263] tissue development,[264] and voltage-gating of ion channels.[265] Piezoelectricity, in particular, has been observed in bone,[266] tendon,[267] teeth,[268] wood,[269] butterfly wings,[270] seashells,[271] fascia,[103] and peptide nanotubes.[71] Biosystems typically present a complex hierarchical structure from the nano- to the macroscale: in fibrillar connective tissues, 300 nm long collagen molecules made of three polypeptide strands self-assemble into fibrils, which in turn are bundled into fibres. The advent of PFM has allowed the piezoelectric nature of individual collagen fibrils to be demonstrated.[272] Furthermore, amino acids, which are the building blocks of proteins, have been shown to be noncentrosymmetric and thus, piezoelectric as well.[273,274] Other forms of electromechanical coupling observed in biological systems include flexoelectricity in lipid membranes[275] and ferroelectricity in aorta tissue.[276] In this context, the application of PFM to the characterisation of biosystems is motivated by the desire to locally probe electromechanical coupling in order to understand the nanoscale origins of related biofunctional phenomena. At the same time, the motivation to study the piezo- and ferroelectric properties of organic molecules and polymers arises also from the need to reduce the use of typically lead-based inorganic ferroelectrics in electronic applications. Organic piezo- and ferroelectric materials represent a versatile, environmentally-friendly alternative to these toxic compounds and are key to the development of biocompatible devices. For example, organic virus-based piezoelectric energy harvesting has been recently demonstrated,[277] and organic ferroelectrics have been employed to increase the energy efficiency of organic solar cells by reducing electron-hole recombination.[42]

5.2 Electromechanical phenomena in organic and biological systems

PFM was first utilised to probe electromechanics in biological systems in 2004 by Halperin *et al.* to answer the question of whether nanoscale piezoelectricity exists in wet and dry human bone.[278] The VPFM response was measured as a function of V_{ac} in order to quantify the longitudinal d_{33} piezoelectric coefficient of bone. A linear dependence of the VPFM response was observed as a function of V_{ac}, as shown in Fig. 9 (b), indicative of piezoelectric coupling. In contrast, a longitudinal piezoresponse cannot be detected using macroscale measurements due to cancelling contributions from differently oriented regions in the bone.[266] Halperin *et al.* reported similar piezoresponse values for dry and wet bone, a result contradictive of macroscopic measurements by Reinish *et al.*, who showed decreased piezoelectricity in wet bone.[279] This decrease has generally been attributed to the uptake of intrafibrillar water. However, piezoelectricity in other collagenous tissues (e.g., cornea and sclera) has been shown to increase with increasing water content,[280–282] highlighting existing discrepancies in the literature between results obtained using macroscale measurements. In this context, locally probing the electromechanical properties of these complex biosystems allows such discrepancies to be resolved by determining the geometrical orientation of the response at the scale of the elements responsible for the piezoelectric behaviour.

Similarly to inorganic materials, the orientation of the piezoresponse can be determined in the coordinate system of the biomaterial, as discussed in Sect. 2.3.4. This orientation mapping was elegantly demonstrated on protein molecules embedded in tooth enamel, as shown in Fig. 10.[270] Both topography and elasticity (Fig. 10 (a) and (b), respectively) of the enamel surface reveal no significant contrast, yet, PFM reveals a hidden structure having both out-of-plane and in-plane piezoelectric components (Fig. 10 (c) and (d), respectively). By employing a vectorial analysisd, it is possible to visualise the 2D (or 3D) electromechanical response data representing both magnitude of piezoresponse and molecular polar orientation, as seen in Fig. 10 (e).[53] Understanding the functionality of biological systems at the nanoscale is possible by combining elastic and piezoelectric AFM measurements, since these properties are intrinsically linked.[270] The ability to map molecular polar orientation at the nanoscale has paved the way for future studies to study electromechanical properties of complex biomolecules, which was previously impossible.

While the performance of inorganic piezo- and ferroelectric materials possessing a high electric polarisation have so far surpassed those of sustainable alternatives,[283,284] there has been in the re-

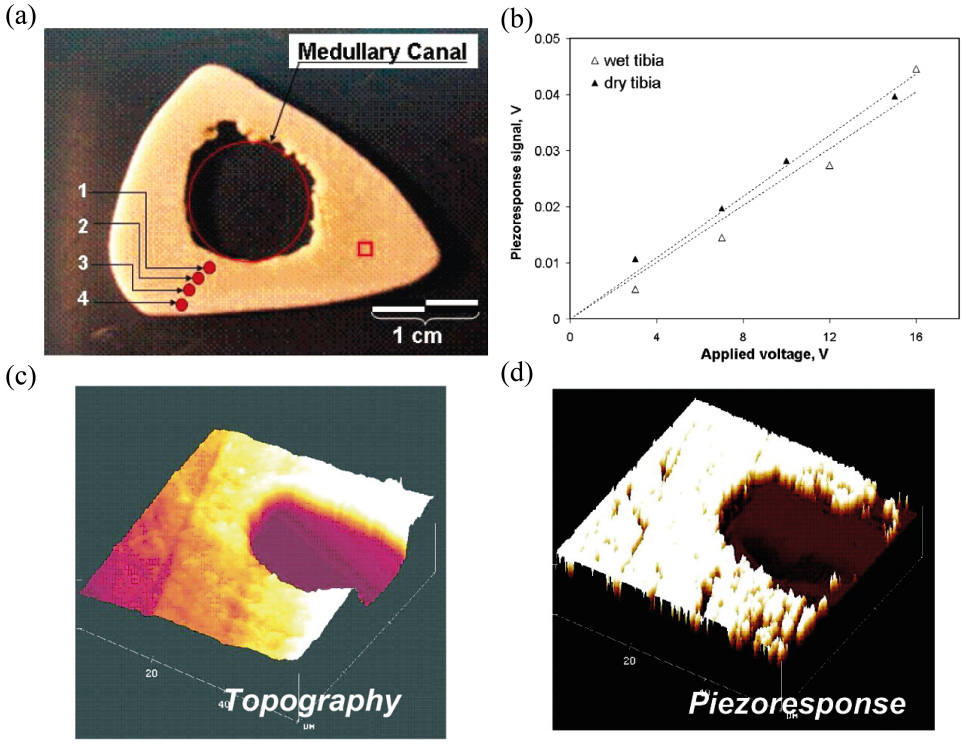

Figure 9: PFM demonstrated on wet and dry human bone. (a) Optical image of transverse cut of bone highlighting the locations of the measured longitudinal piezoelectric coefficients. (b) Longitudinal piezoelectric response measured on wet and dry bone. (c) Topography AFM image rendered in 3D of cross-section of human bone. (d) VPFM image of bone in the area of the Haversian canal (region of low response). Reprinted with permission from Halperin *et al.*,[278] copyright 2004, American Chemical Society.

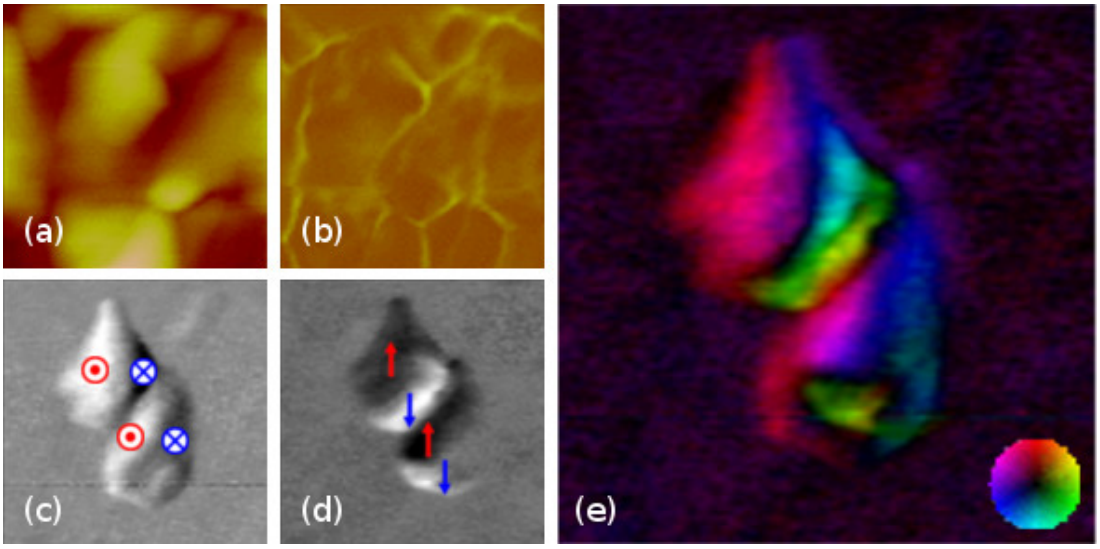

Figure 10: PFM study of protein molecules in tooth enamel. (a) Surface topography and (b) elasticity image of the enamel surface. (c) VPFM and (d) LPFM images of the same region. (e) Vector PFM map representing the local electromechanical response, where the colour indicates the molecular orientation direction and the intensity indicates the magnitude of electromechanical response. The image size is 400 nm. Adapted with permission from Kalinin *et al.*,[270] copyright 2005, Elsevier B.V.

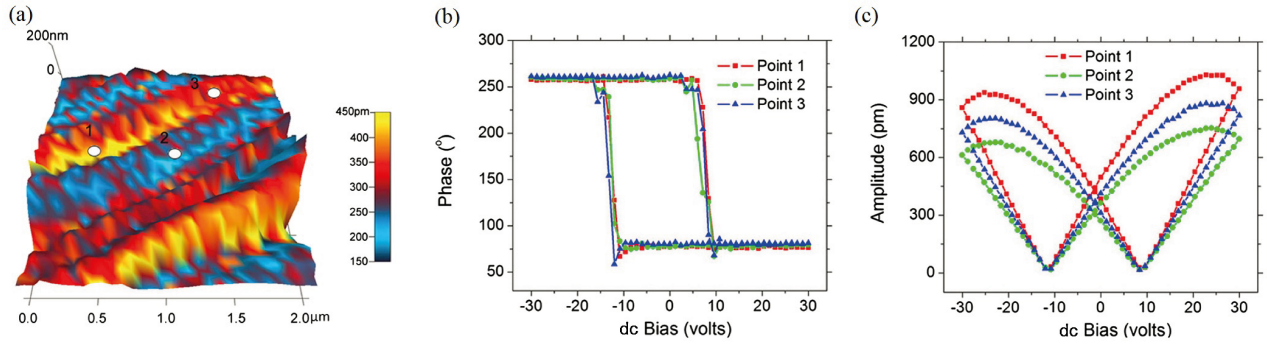

Figure 11: Ferroelectric switching of the inner aortic wall via SS-PFM. (a) SS-PFM map of remnant PFM amplitude with three locations marked. (b) Phase-voltage loop and (c) amplitude-voltage hysteresis loop measured on three locations on the aortic wall. Reprinted with permission from Liu *et al.*,[276] copyright 2012, American Physical Society.

cent years a significant increase in the number of reported organic materials[285] with comparably high polarisation, and even, in some cases, ferroelectricity.[286] Examples include croconic acid,[287] peptide nanostructures,[71] imidazoles,[288] and polyvinylidene fluoride (PVDF).[256,289,290] Diphenylalanine peptide nanostructures have been studied with PFM and shown to possess a high shear piezoelectric constant(d_{15} = 60 pm/V)[71] as well as evidence of ferroelectricity.[291] In addition, this material is biocompatible and possesses a high mechanical stability and stiffness.[292] The ability of diphenylalanine peptides to self-assemble into various structures,[293,294] including nanotubes, fibrils, scaffolds, and hydrogels, increases its attraction for a wide range of applications, including biosensing and tissue engineering.[293] PFM has also been used to study the piezoelectric, ferroelectric, and relaxation behaviour of the copolymer PVDF and trifluoroethylene TrFE, [P(VDF-TrFE)],[290,295] which has already been used in field effect transistors[296] and shows great promise for potential use in organic electronic devices.

5.3 Ferroelectric phenomena in organic and biological systems

Ferroelectricity has been studied in detail in inorganic compounds (see Sect. 3). It is only recently that this ferroelectric behaviour has been reported for organic biosystems, such as shell nacre,[297] aorta wall,[276] and crystalline glycine.[298] The role ferroelectricity may play in the aorta was hypothesised by Chen and Gao to serve as a force sensor to maintain blood pressure homeostasis, or even to serve as a local integrated memory-like structure integrated with surrounding nerves.[299] Indeed ferroelectric behaviour has been reported in many organic systems, including smectic liquid crystals consisting of banana shaped achiral molecules,[300] as well as antiferroelectric behaviour in amphiphilic glycolipid molecules in bent-core liquid crystals.[301] In such systems, the presence of a switchable polarisation has been investigated using PFM. In particular, Liu *et al.* reported ferroelectric behaviour in the aorta wall using SS-PFM.[276] Three representative phase- and amplitude-voltage loops are shown in Fig. 11. The phase-voltage hysteresis loop shows a phase difference of $\approx 180°$ and corresponding amplitude-voltage hysteresis loops, typically associated with ferroelectric behaviour (Fig. 11 (b) and (c)). In a subsequent study, PFM and SS-PFM have been used to attribute the piezo- and ferroelectric behaviour of aorta to elastin fibrils.[302] The authors also discovered that the ferroelectric nature of elastin is suppressed partially, or in some cases completely, by the presence of glucose.[302] These results indicate that ferroelectricity, or lack thereof, could be coupled to glycation of elastin, which is connected to aging[303] and several diseases such as diabetic macroangiopathy.[304] Similar results using SS-PFM were demonstrated in crystalline γ-glycine[298] and seashells;[297] however, the origin and biofunctional role of ferroelectric-like behaviour in biomaterials remain topics of discussion (see Sect. 6).

The organic copolymer P(VDF-TrFE) was the first ferroelectric sample investigated by PFM.[26,27] Since then, researchers have investigated the local polarisation structure and switching in a wide variety of P(VDF-TrFE) structures, including films,[289] nanomesas,[290,305] and nanotubes.[306] A PFM and SS-PFM study[289] demonstrated the possibility to write and erase polarisation domains having

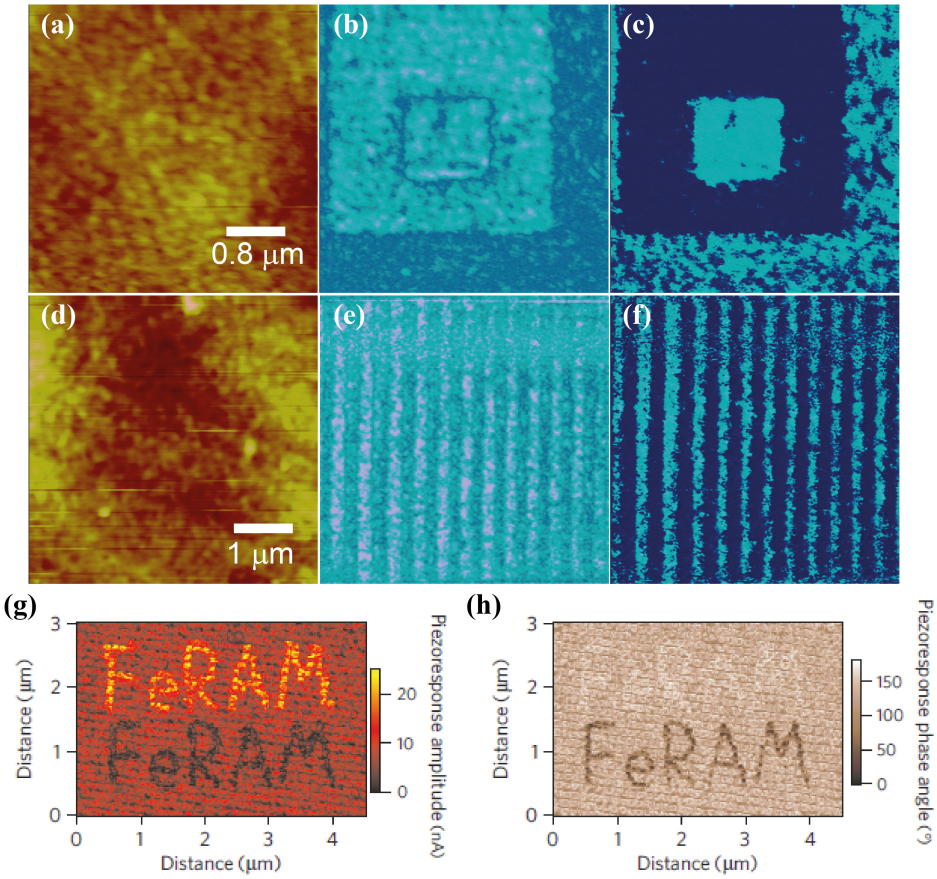

Figure 12: VPFM images of written domains using biased tip (±10 V) in a thin film P(VDF-TrFE 70:30) copolymer. (a),(d) Topography; (b),(e) VPFM amplitude; (c),(f) VPFM phase. VPFM images of switching in P(VDF-TrFE) nanostructures. (g) VPFM amplitude and (h) VPFM phase after switching the word "FeRAM" in the nanostructure array. Reprinted with permission from Rodriguez *et al.*,[289] copyright 2007, American Institute of Physics, and Hu *et al.*,[295] copyright 2008, Nature Publishing Group.

a width as low as 25 nm in P(VDF-TrFE) thin films, revealing their applicability in the field of organic ferroelectrics. In Fig. 12, PFM images of P(VDF-TrFE) films are displayed after poling two square areas in the film (10 V and -10 V), which show evidence of ferroelectric switching in the film. Ferroelectricity had been shown in this manner previously,[26] however, as seen in Fig. 12 (e) and (f), it was possible for the authors to use a bipolar square wave bias to pole parallel domains with a resolution limited only by the grain size inherent in the film, suggesting the viability of such films for use in high density storage devices. Hu *et al.* later demonstrated the production of regular nanostructure arrays of P(VDF-TrFE) via a nano-imprinting process.[295] The bright letters were poled into the nanostructures using a positive (5 V) bias, whereas dark letters were poled using a negative bias (-5 V), as shown in the subsequent PFM amplitude and phase images (Fig. 12 (g) and (h), respectively). The fabrication process used improved the crystal orientation in each nanostructure, which resulted in lower energy losses and a lower coercive field than previously reported bulk values.[307] In the past five years, the domain writing and switching properties of P(VDF-TrFE) thin films have been the focus of several PFM and SS-PFM studies using similar protocols as described in Sect. 3.4.[308] Several important differences with respect to inorganic crystalline ferroelectrics have been highlighted, including more irregular domain shapes, nucleation of domains away from the AFM tip,[309] and highly nonuniform domain wall velocity characterised by a low creep exponent.[310]

5.4 Outlook

Given the ubiquity and variety of electromechanical phenomena, in particular piezoelectricity, in organic systems, there likely remains a vast range of biomaterials to be investigated at the nanoscale. While organic piezo- and ferroelectrics with increasingly high polarisation are being discovered and proposed as sustainable alternatives to lead-based compounds,[285,286] there is a large scope for understanding the nanoscopic origins and biofunctional implications of electromechanical coupling in natural tissues. In cell research, the surface roughness, chemistry, and mechanical properties of synthetic biomaterials such as aligned collagen matrices[311,312] have been extensively researched to serve as microenvironments that can be tailored to elicit specific cell responses.[313–315] In contrast, the possible role played by piezoelectricity and electrical charging in these materials on cell behaviour remains largely unexplored. Furthermore, while electroactivity and even piezoelectricity[316] have been reported in certain types of cells, PFM has to this day found very limited application to cells.

Biomaterials can present challenges in PFM experiments due to their intrinsic complex hierarchical structure spanning many length scales and relatively small piezoresponse with respect to inorganic ferroelectrics. Liquid PFM, in particular, is not widely used, despite having been demonstrated on model ferroelectric systems.[55,102,159] A possible reason for this could be the observed signal reduction in the piezoresponse of model ferroelectrics in solutions approaching physiological conditions.

6 PFM applied to nonpiezoelectric materials

Given the breadth of different materials exhibiting electromechanical coupling, it is important to consider the range of voltage-sensitive mechanisms that can contribute to a strain response, detectable by PFM but not necessarily piezoelectric in nature. Examples include ionic and electronic transport,[317] electrostriction,[318] Joule heating,[318] electrochemical effects,[24] flexoelectricity,[319] and electrostatic interactions.[78] A particularly striking example is the report of a ferroelectric-like switching behaviour in $LaAlO_3/SrTiO_3$ heterostructures by Bark *et al.*,[222] in which purely electrostatic contributions were ruled out by complementary EFM measurements and the changes in bulk polarity of the $LaAlO_3$ layer were attributed to oxygen vacancy migration reversibly switching between two bistable configurations.

An AFM technique developed to probe electrochemical strain-responses in voltage-sensitive materials is ESM.[24] In ESM, the applied electric field leads to a local change of ion concentration underneath the tip, thus generating a local strain, which is detectable by the resultant tip deflection. This technique can be applied to systems that generate an ionic current and/or chemical reactions in response to an applied voltage, such as intercalation-deintercalation reactions in Li-ion batteries.[24,25] Modelling of the electromechanical response in solid electrolytes in ESM was conducted recently by Tselev *et al.*, who showed that ESM image formation originates from the top layer of the surface (even a one-unit-cell thick layer at the surface will dominate the ESM signal).[320] Eliseev *et al.* demonstrated that electrostriction dominates the signal in PFM and ESM measurements in materials with a low dielectric constant in the presence of a dielectric gap of only 1 unit-cell thickness.[80] This high surface sensitivity shows rigorous analysis is needed when interpreting ESM and PFM signals since, in addition, ionic and electrochemical phenomena can play a significant role in the electromechanical properties of, e.g., oxides.[321] Another recently-developed AFM technique, first-order reversal curve current-voltage, by Strelcov *et al.*[322] allows for the separation of ionic and electrical processes and can be used in tandem with PFM or ESM to discriminate between piezoelectricity and other phenomena. Recent investigations have revealed ferroelectric-like behaviour in nonpiezoelectric materials such as glass,[323] silicon,[324] and even banana peel,[325,326] showing that the origin of voltage-generated strains at the nanoscale measured by PFM may not be entirely piezo- or ferroelectric in origin, but can result from other phenomena. More worryingly, materials that are often used as a substrate for thin film samples such as silicon,[324] and $SrTiO_3$[327] have shown ferroelectric-like behaviour using PFM. In this Section, guidelines are provided on how to use a combination of time-resolved PFM and ESM to decouple ferroelectric-like behaviour from actual piezo- and ferroelectricity.

Until recently, one of the benchmarks for proving nanoscale ferroelectricity in materials was based on obtaining a hysteresis loop using SS-PFM.[106] Obtaining loops and measuring subsequent displacements is equivalent for PFM and ESM. Recently, Proksch[323] applied SS-PFM to soda-lime glass (an

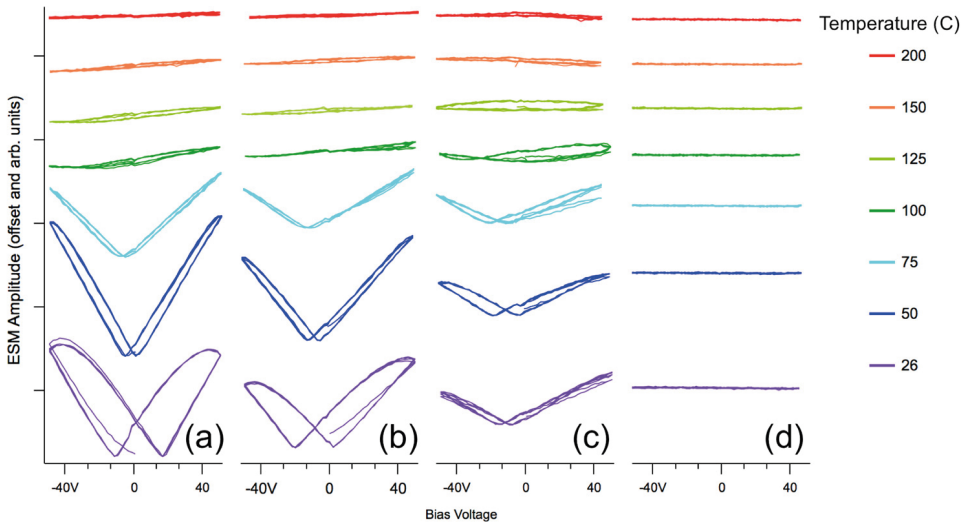

Figure 13: Comparison of hysteretic behaviour induced by cationic diffusion in soda lime glass and fused silica. ESM amplitude loops versus bias voltage (-50 V to 50 V) as a function of temperature for (a) soda-lime glass - Pt tip, (b) soda-lime glass - Ir tip, (c) soda-lime glass having lower cation concentration than in (a) and (b) - Pt tip, and (d) fused silica - Pt tip. Reprinted with permission from Proksch,[323] copyright 2014, American Institute of Physics.

amorphous network of SiO_2 with a high concentration of cations) and fused silica (containing a very low cation concentration) as a function of temperature for two different cantilever coatings (Pt and Ir). Amplitude loops of each sample recorded from room temperature (RT) to 200°C are shown in Fig. 13. ESM loops of the high cation soda-lime glass are shown in Fig. 13 (a), where typical ferroelectric amplitude butterfly loops are observed at RT as a result of electrochemical strain resulting from temperature-dependent cationic diffusion processes. ESM loops of fused silica, however, show no hysteretic behaviour, as can be seen in Fig. 13 (d). These results prove that a hysteresis can be observed for materials subject to cationic diffusion. Clearly, the water layer influences these measurements since hysteretic behaviour disappears as the temperature is increased to 200°C in the case of the soda-lime glasses (Fig. 13 (a)-(c)). Another interesting result from this study is the change in the hysteretic shape of the amplitude loops of the same sample (high cation soda-lime) depending on the metal coating of the tip; the ESM response is higher when a Pt coating is used, corresponding to the higher electro-catalytic activity of Pt. A similar study has been conducted on Si,[324] where amplitude and phase loops characteristic of ferroelectric switching were obtained, and a ferroelectric-like behaviour, electrochemical in nature, persisted after mounting nonferroelectric samples on Si. An ESM study by Kim *et al.* on paraelectric thin films of $SrTiO_3$ and TiO_2 also showed evidence of nanoscale ferroelectric-like behaviour.[328] A time-resolved study was conducted using dynamic ESM (D-ESM), exploring the relaxation of the electromechanical signal after the application of a dc bias, as shown in Fig. 14. The loops are reminiscent of ferroelectric relaxors, yet KPFM studies on both thin films revealed changes in surface potential via charge injection. Thus, Kim *et al.* attributed ionic processes to the observed hysteretic and ferroelectric-like behaviour.

To explore the mechanisms behind electromechanical coupling, Chen *et al.* investigated three systems using SS-PFM: ferroelectric polycrystalline PZT, a lithium iron phosphate film with large Vegard strain (local lattice deformations arising from defects and vacancies), and soda-lime glass.[329] Fig. 15 shows the SS-PFM amplitude and phase responses for the three materials: PZT shows the expected ferroelectric behaviour, with a characteristic amplitude butterfly loop and 180° phase shift. Since lithium iron phosphate is a nonpolar ionic system, an applied dc voltage should invoke a strain response, observed in the flat phase response in Fig. 15 (b). However, similarly to the study by Proksch, the soda-lime glass exhibits the typical ferroelectric signature of an amplitude butterfly loop and 180° phase shift. The SS-PFM phase response of the soda-lime glass is evidence of dipolar behaviour, but not necessarily ferroelectric behaviour. Further investigations by Chen *et al.* have aimed to distinguish between spontaneous and induced polarisation and involved recording both the first and second

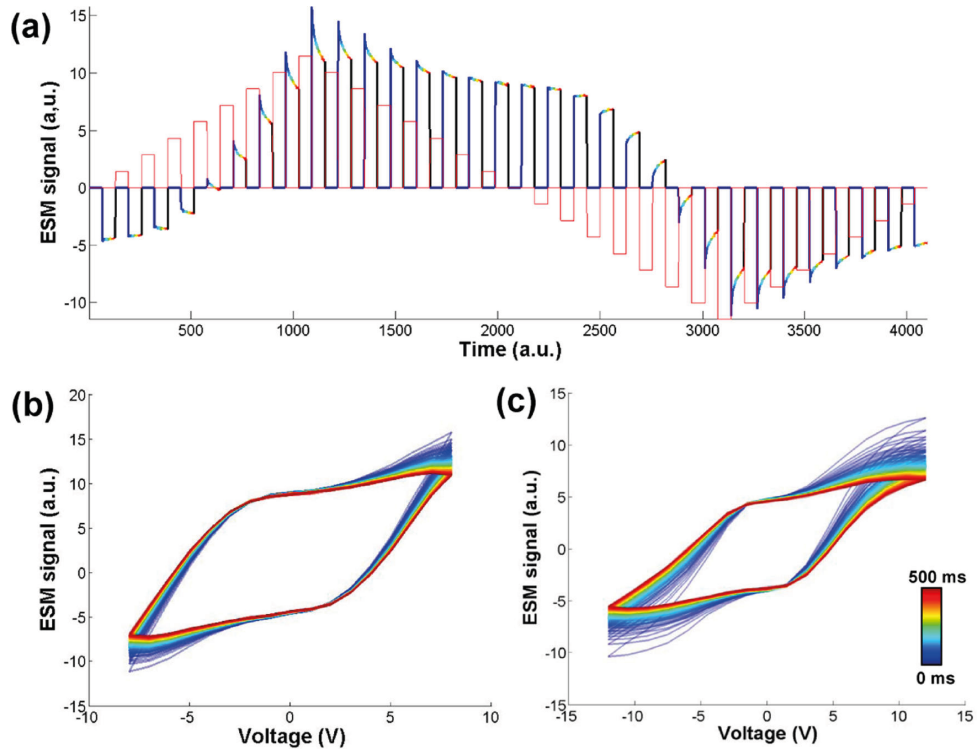

Figure 14: Time-dependent study using D-ESM. (a) Outer envelope of a triangular waveform in a D-ESM measurement overlaid on the measured time-dependence of the ESM response recorded from the $SrTiO_3$ thin films. D-ESM loops as a function of time delay, illustrating relaxation dynamics for different maximum applied voltages in (b) $SrTiO_3$ and (c) TiO_2 thin films. Reproduced with permission from Kim *et al.*,[328] copyright 2012, American Chemical Society.

harmonic PFM responses, which are related to the piezoelectric and electrostrictive properties of the material, respectively. Classical ferroelectrics generally have a large spontaneous polarisation, where the strain is linear with the applied ac voltage. However, materials having a large induced polarisation compared to the spontaneous polarisation have a strain predominantly quadratic as a function of the applied ac voltage.[330] Results from this study showed a significantly higher second harmonic response for soda-lime glass compared to PZT, indicating that the voltage-induced strain in soda-lime is predominantly due to an induced polarisation. Combining VPFM and LPFM also distinguished between PZT and the soda-lime glass, since vertical and lateral piezoreponses on polycrystalline PZT have a similar amplitude; in contrast, induced dipoles in the amorphous soda-lime glass align along the applied electric field direction, leading to a very low lateral response.

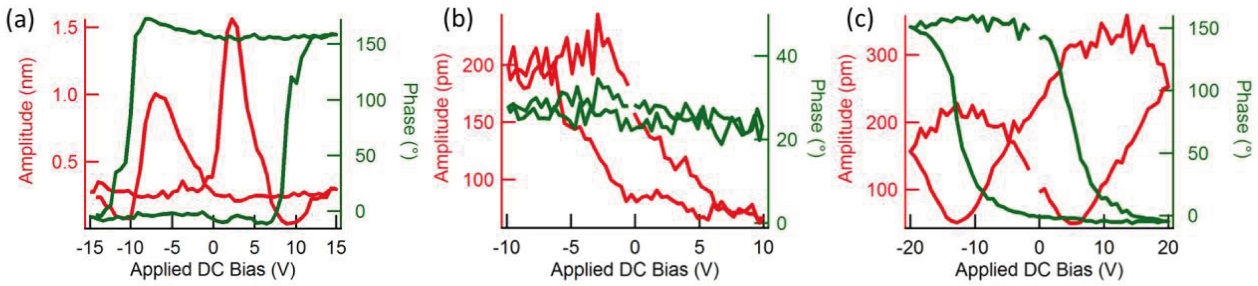

Figure 15: Phase-voltage and amplitude-voltage loops of three representative material systems: (a) PZT; (b) lithium iron phosphate; and (c) soda-lime glass. Reprinted with permission from Chen *et al.*,[329] copyright 2014, American Institute of Physics.

6.1 Outlook

The studies presented in this Section highlight the importance of decoupling electromechanical and induced ionic transport phenomena through combined PFM and ESM measurements. This ability is important in investigations of the presence of ferroelectricity in a material in order to identify the origin of a hysteretic behaviour. More importantly, the combination of PFM, ESM, and other AFM techniques opens the door to investigate electronic and ionic phenomena at the nanoscale in a much wider range of materials, beyond piezoelectrics. In particular, conductive-AFM can be used in complement to ESM to characterise the differences and/or correlation between electronic and ionic transport in fuel cells.

We finally highlight the recent discovery of piezoelectric behaviour in two-dimensional materials,[331] which has sparked much interest for stretchable and miniaturised deviced. Density functional theory was used to show the possibility of inducing piezoelectricity in centrosymmetric graphene through the introduction of tailored porosity[332] and the selective adsorption of atoms.[333,334] Similarly, despite the centrosymmetric structure of bulk 2D boron nitride and transition metal dichalcogenide crystals (e.g., MoS2), single monolayers are non-centrosymmetric, prompting Duerloo *et al.* to calculate the piezoelectric properties of such 2D materials using DFT.[335,336] Some structural configurations of graphene oxide have been reported to be piezoelectric as well, based on DFT calculations.[337] Wu et al. provided experimental evidence of piezoelectricity in single and odd layers of MoS_2 via the direct piezoelectric effect, measuring current under strain.[338] Most recently, Zelisko *et al.* used PFM to observe piezoelectricity in 2D graphene nitride.[339]

7 Conclusions

PFM has advanced current understanding of electromechanical phenomena in a wide range of piezoelectric and nonpiezoelectric materials alike, as highlighted by the broad scope of this review, with each material bringing new challenges and opportunities. Issues remain in terms of quantification of voltage-induced surface displacements, attribution of the measured displacements to the appropriate phenomenon, and quantification of piezoelectric coefficients, which requires appropriate calibration of the detection system. Clearly, understanding and elucidating the assumptions made in a PFM experiment and identifying best practices for minimising artefacts will continue to benefit the community in the long term, allowing users to fully exploit future developments in instrumentation and techniques.

Ferroelectric materials have largely been the driving force for the continued development and wide adoption of PFM, and in turn, PFM has provided a unique characterisation tool for probing nano- to microscale ferroelectric properties, shedding light on, e.g., ferroelectric switching in the vicinity of defects,[340] the role of polar nanoregions on the properties of ferroelectric relaxors,[341] and exploring the applications of domain wall nanoelectronics.[121] PFM has been shown to elucidate electromechanical functionality in ferroelectric and piezoelectric semiconductors, and will certainly continue to be utilised with the advent of piezoelectric nanogenerators for energy harvesting applications.

The application of PFM to biosystems with their typically hierarchical, multiphase structure has opened the door to investigate the structure-function relationship of any electromechanically-responsive biosystems at the nanoscale. PFM has also been used to visualise polar order in collagenous tissues at the nanoscale, revealing a complex naturally occurring polar architecture, which cannot be detected using standard electron or optical (e.g., fluorescence) microscopy, or by simple AFM topography.[342] Similarly, the use of organic piezo- and ferroelectrics in conventional and flexible electronics applications can be enabled by PFM. Already organic ferroelectrics are being used in solar cells[42] and field effect transistors,[296] and are a promising alternative to inorganic ferroelectrics because of their lower production costs and environmentally-friendly composition.

The demonstration of ferroelectric-like behaviour in nonferroelectric materials has sparked intensive research into better understanding the origins of electromechanical phenomena measured using PFM and ESM. Many mechanisms can contribute to strain in a voltage-sensitive material, such as ionic, electrochemical, electrostatic, and electrostrictive phenomena, which are all detectable in PFM and ESM. However, through time-resolved PFM and ESM, comparison of vertical and lateral PFM components, and by investigating higher harmonics of the PFM and ESM signals, it is possible to decouple ionic, induced polarization, and piezoelectric properties in AFM.

Over the past two decades, improvements in PFM instrumentation and data acquisition have led to the implementation of a variety of spectroscopic waveforms for probing and gaining insight into, e.g., ferroelectric switching, via the generation and analysis of highly multidimensional datasets.[343] Increasingly, PFM is being used as one of many tools in a toolbox to probe structure and function across multiple length scales, and the necessity of integrating, analysing, and correlating data from multiple complementary techniques is apparent, often requiring 'deep data analysis',[344,345] ideally via the coordination of theoretical modelling and experimental approaches. In parallel to these improvements, the scope of PFM and related techniques has now extended to materials well beyond ferroelectrics and even piezoelectrics, effectively becoming an accessible nanoscale probe of electronic and ionic phenomena alike. It is therefore very likely that the already broad applicability of PFM in materials research will continue to expand in the upcoming years.

Acknowledgements

This publication has been made possible with the financial support of Science Foundation Ireland under grant number SFI10/RFP/MTR2855 and the Swiss National Science Foundation under grant number P2GEP2_151809. The authors gratefully acknowledge Dr. J. I. Kilpatrick and S. Neumayer for assistance with Sect. 2.

References

[1] A. Meitzler, H. F. Tiersten, A. W. Warner, D. Berlincourt, G. A. Couqin, and F. S. Welsh. IEEE standard on piezoelectricity, 1988.

[2] M. E. Lines and A. M. Glass. *Principles and Applications of Ferroelectrics and Related Materials*. Clarendon press Oxford, Oxford, Great Britain, 2001.

[3] N. Setter, D. Damjanovic, L. Eng, G. Fox, S. Gevorgian, S. Hong, A. Kingon, H. Kohlstedt, N. Y. Park, G. B. Stephenson, I. Stolichnov, A. K. Tagantsev, D. V. Taylor, T. Yamada, and S. Streiffer. *J. Appl. Phys.*, 100:051606, 2006.

[4] M. L. Dunn. *J. Appl. Phys.*, 78:1533, 1995.

[5] Y. L. Wang, Tagantsev A. K., Damjanovic D., and Setter N. *Appl. Phys. Lett.*, 91:062905, 2007.

[6] N. Bassiri-Garb, I. Fuji, E. Hong, S. Trolier-McKinstry, D. V. Taylor, and D. Damjanovic. *J. Electroceram.*, 19:49, 2007.

[7] S. B. Seshadri, A. D. Prewitt, A. J. Studer, D. Damjanovic, and J. L. Jones. *Appl. Phys. Lett.*, 102:042911, 2013.

[8] A. Roelofs, I. Schneller, K. Szot, and R. Waser. *Appl. Phys. Lett.*, 81:5231, 2002.

[9] A. Roelofs, I. Schneller, K. Szot, and R. Waser. *Nanotechnology*, 14:250, 2003.

[10] C. Lichtensteiger, M. Dawber, and J.-M. Triscone. Ferroelectric size effects. In K. M. Rabe, C. H. Ahn, and J.-M. Triscone, editors, *Physics of Ferroelectrics: a Modern Perspective*, pages 305–337. Springer, Berlin, 2007.

[11] A. Rüdiger and R. Waser. *J. Alloys Compd.*, 449:2, 2008.

[12] Y. Bastani, T. Schmitz-Kempen, A. Roelofs, and N. Bassiri-Gharb. *J. Appl. Phys.*, 109:014115, 2011.

[13] B. J. Rodriguez, R. Proksch, P. Maksymovych, and S. V. Kalinin. *Scanning Probe Microscopy – Forces and Currents in the Nanoscale World*, pages 539–614. Wiley-VCH Verlag GmbH & Co. KGaA, Weinheim, 2012.

[14] G. Binnig, C. Quate, F. Calvin, and C. Gerber. *Phys. Rev. Lett.*, 56:930, 1986.

[15] E. Meyer, H. J. Hug, and R. Bennewitz. *Scanning probe microscopy: the lab on a tip.* Springer, Berlin, 2004.

[16] D. A. Bonnell. *Scanning probe microscopy and spectroscopy: theory, techniques, and applications.* Wiley-VCH, Weinheim, 2001.

[17] S. V. Kalinin and A. Gruverman. *Scanning probe microscopy: electrical and electromechanical phenomena at the nanoscale*, volume 1. Springer, Berlin, 2007.

[18] L. Gross. *Nat. Chem.*, 3:273, 2011.

[19] Y. Martin and H. K. Wickramasinghe. *Appl. Phys. Lett.*, 50:1455, 1987.

[20] M. Nonnenmacher, M. P. O'Boyle, and H. K. Wickramasinghe. *Appl. Phys. Lett.*, 58:2921, 1991.

[21] Noy A, C. D. Frisbie, L. F. Rozsnyaiand, M. S. Wrighton, and C. M. Lieber. *J. Am. Chem. Soc.*, 117:7943, 1995.

[22] A. Gruverman and A. L. Kholkin. *Rep. Prog. Phys.*, 69:2443, 2006.

[23] S. V. Kalinin, A. N. Morozovska, L. Q. Chen, and B. J. Rodriguez. *Rep. Prog. Phys.*, 73:056502, 2010.

[24] N. Balke, S. Jesse, A. N. Morozovska, E. Eliseev, D. W. Chung, Y. Kim, L. Adamczyk, R. E. Garcia, N. Dudney, and S. V. Kalinin. *Nature Nanotech.*, 5:749, 2010.

[25] N. Balke, S. Jesse, Y. Kim, L. Adamczyk, A. Tselev, I. N. Ivanov, N. J. Dudney, and S. V. Kalinin. *Nano Lett.*, 10:3420, 2010.

[26] P. Güthner and K. Dransfeld. *Appl. Phys. Lett.*, 61:1137, 1992.

[27] P. Güthner, J. Glatz-Reichenbach, and K. Dransfeld. *J. Appl. Phys.*, 69:7895, 1991.

[28] H. Birk, J. Glatz-Reichenbach, L. Jie, E. Schreck, and K. Dransfeld. *J. Vac. Sci. Technol., B*, 9:1162, 1991.

[29] K. Franke, J. Besold, W. Haessler, and C. Seegebarth. *Surf. Sci.*, 302:L283, 1994.

[30] T. Hidaka, T. Maruyama, M. Saitoh, N. Mikoshiba, M. Shimizu, T. Shiosaki, L. A. Wills, R. Hiskes, S. A. Dicarolis, and J. Amano. *Appl. Phys. Lett.*, 68:2358, 1996.

[31] A. Gruverman, O. Auciello, and H. Tokomuto. *J. Vac. Sci Technol.*, 14:602, 1996.

[32] A. Gruverman, O. Auciello, and H. Tokumoto. *Appl. Phys. Lett.*, 69:3191, 1996.

[33] T. Hidaka, T. Maruyama, I. Sakai, M. Saitoh, L. A. Wills, R. Hiskes, S. A. Dicarolis, J. Amano, and C. M. Foster. *Integr. Ferroelectrics*, 17:319, 1997.

[34] G. Zavala, J. H. Fendler, and S. Trolier-McKinstry. *J. Appl. Phys.*, 81:7480, 1997.

[35] T. Tybell, C. Ahn, and J.-M. Triscone. *Appl. Phys. Lett.*, 72:1454, 1998.

[36] O. Auciello, A. Gruverman, H. Tokumoto, S. A. Prakash, S. Aggarwal, and R. Ramesh. *MRS Bull.*, 23:33, 1998.

[37] M. Abplanalp, L. M. Eng, and P. Günter. *Appl. Phys. A: Mater. Sci. Process.*, 66:S231, 1998.

[38] L. M. Eng, M. Abplanalp, and P P. Günter. *Appl. Phys. A: Mater. Sci. Process.*, 66:S679, 1998.

[39] J. F. Scott and C. A. Paz de Araujo. *Science*, 246:1400, 1989.

[40] R. Waser and A. Rüdiger. *Nature Mater.*, 3:81, 2004.

[41] A. Chanthbouala, V. Garcia, R. O. Cherifi, K. Bouzehouane, S. Fusil, X. Moya, S. Xavier, H. Yamada, C. Deranlot, N. D. Mathur, M. Bibes, A. Barthélémy, and J. Grollier. *Nature Mater.*, 11:860, 2012.

[42] Y. Yuan, T. J. Reece, P. Sharma, S. Poddar, S. Ducharme, A. Gruverman, Y. Yang, and J. Huang. *Nature Mater.*, 10:296, 2011.

[43] R. Nechache, C. Harnagea, S. Li, L. Cardenas, W. Huang, J. Chakrabartty, and F. Rosei. *Nature Photon.*, 9:61, 2014.

[44] Y. Kutes, L. Ye, Y. Zhou, S. Pang, B. D. Huey, and N. P. Padture. *J. Phys. Chem. Lett.*, 5:3335, 2014.

[45] S. V. Kalinin and A. L. Kholkin. *J. Appl. Phys.*, 110:051901, 2011.

[46] J. Li, S. V. Kalinin, and A. L. Kholkin. *J. Appl. Phys.*, 113:187101, 2013.

[47] N. Bassiri-Gharb, S. V. Kalinin, and N. Valanoor. *J. Appl. Phys.*, 116:066701, 2014.

[48] A. Gruverman, O. Auciello, and H. Tokumoto. *Annu. Rev. Mater. Sci.*, 28:101, 1998.

[49] A. Gruverman. Ferroelectric nanodomains. In H. S. Nalwa, editor, *Encyclopedia of Nanoscience and Nanotechnology*, volume 3, pages 359–375. American Scientific Publishers, Los Angeles, 2004.

[50] A. Gruverman and M. Alexe. *Nanoscale Characterization of Ferroelectric Materials.* Springer, Berlin, 2004.

[51] S. Hong. *Nanoscale phenomena in ferroelectric thin films.* Springer, New York, 2004.

[52] A. Gruverman and S. V. Kalinin. *J. Mater. Sci.*, 41:107, 2006.

[53] S. V. Kalinin, B. J. Rodriguez, S. Jesse, J. Shin, A. P. Baddorf, P. Gupta, H. Jain, D. B. Williams, and A. Gruverman. *Microsc. Microanal.*, 12:206, 2006.

[54] S. V. Kalinin, A. Rar, and S. Jesse. *IEEE Trans. on Ultrasonics, Ferroelectrics and Frequency Control*, 53:2226, 2006.

[55] S. V. Kalinin, S. Jesse, B. J. Rodriguez, K. Seal, A. P. Baddorf, T. Zhao, Y. H. Chu, R. Ramesh, E. A. Eliseev, A. N. Morozovska, B. Mirman, and E. Karapetian. *Jpn. J. Appl. Phys.*, 46:5674, 2007.

[56] S. V. Kalinin, B. J. Rodriguez, S. Jesse, E. Karapetian, B. Mirman, E. A. Eliseev, and A. N. Morozovska. *Annu. Rev. Mater. Res.*, 37:189, 2007.

[57] A. L. Kholkin, I. K. Bdikin, D. A. Kiselev, V. V. Shvartsman, and S.-H. Kim. *J. Electroceram.*, 19:81, 2007.

[58] D. A. Bonnell, S. V. Kalinin, A. L. Kholkin, and A. Gruverman. *MRS Bull.*, 34:648, 2009.

[59] N. Balke, I. Bdikin, S. V. Kalinin, and A. L. Kholkin. *J. Am. Ceram. Soc.*, 92:1629, 2009.

[60] E. Soergel. *J. Phys. D: Appl. Phys*, 44:464003, 2011.

[61] X.-H. Du, U. Belegundu, and K. Uchino. *Jpn. J. Appl. Phys.*, 36:5580, 1997.

[62] S. V. Kalinin, E. Karapetian, and M. Kachanov. *Phys. Rev. B*, 70:184101, 2004.

[63] A. Labuda and R. Proksch. *Appl. Phys. Lett.*, 106:253103, 2015.

[64] S. L. Lei, E. A. Eliseev, A. N. Morozovska, R. C. Haislmaier, T. T. A. Lummen, W. Cao, S. V. Kalinin, and V. Gopalan. *Phys. Rev. B*, 86:134115, 2012.

[65] A. V. Ievlev, D. O. Alikin, A. N. Morozovska, O. V. Varenyk, E. A. Eliseev, A. L. Kholkin, V. Ya. Shur, and S. V. Kalinin. *ACS Nano*, 9:769, 2015.

[66] S. V. Kalinin and D. A. Bonnell. *Phys. Rev. B*, 65:125408, 2002.

[67] N. P. D'Costa and J. H. Hoh. *Rev. Sci. Instrum.*, 66:5096, 1995.

[68] M. J. Higgins, R. Proksch, J. E. Sader, M. Polcik, S. McEndoo, J. P. Cleveland, and S. P. Jarvis. *Rev. Sci. Instrum.*, 77:013701, 2006.

[69] Z. Huang, Q. Zhang, S. Corkovic, R. Dorey, and R. W. Whatmore. *IEEE Trans. on Ultrasonics, Ferroelectrics and Frequency Control*, 53:2287, 2006.

[70] R. T. Smith and F. S. Welsh. *J. Appl. Phys.*, 42:2219, 1971.

[71] A. L. Kholkin, N. Amdursky, I. K. Bdikin, E. Gazit, and G. Rosenman. *ACS Nano*, 4:610, 2010.

[72] F. Johann, T. Jungk, M. Lilienblum, A. Hoffmann, and E. Soergel. *Appl. Phys. Lett.*, 97:102902, 2010.

[73] F. Peter, A. Rüdiger, R. Waser, K. Szot, and B. Reichenberg. *Rev. Sci. Instrum.*, 76:046101, 2005.

[74] F. Peter, A. Rüdiger, K. Szot, R. Waser, and B. Reichenberg. *IEEE Trans. on Ultrasonics, Ferroelectrics and Frequency Control*, 53:2253, 2006.

[75] H. Choi, S. Hong, and K. No. *Rev. Sci. Instrum.*, 82:113706, 2011.

[76] S. V. Kalinin and A. Gruverman. *Scanning Probe Microscopy of Functional Materials*. Springer, New York, USA, 2011.

[77] P. L. T. M. Frederix, M. R. Gullo, T. Akiyama, A. Tonin, N. F. de Rooij, U. Staufer, and A. Engel. *Nanotechnology*, 16:997, 2005.

[78] N. Balke, P. Maksymovych, S. Jesse, I. I. Kravchenko, Q. Li, and S. V. Kalinin. *ACS Nano*, 8:10229, 2014.

[79] A. V. Ievlev, A. N. Morozovska, V. Ya. Shur, and S. V. Kalinin. *Appl. Phys. Lett.*, 94:032907, 2009.

[80] E. A. Eliseev, A. N. Morozovska, A. V. Ievlev, N. Balke, P. Maksymovych, A. Tselev, and S. V. Kalinin. *Appl. Phys. Lett.*, 104:232901, 2014.

[81] D. Dahan, M. Molotskii, G. Rosenman, and Y. Rosenwaks. *Appl. Phys. Lett.*, 89:152902, 2006.

[82] S. Bühlmann, E. Colla, and P. Muralt. *Phys. Rev. B*, 72:214120, 2005.

[83] Y. Kim, S. Buhlmann, S. Hong, S.-H. Kim, and K. No. *Appl. Phys. Lett.*, 90:072910, 2007.

[84] A. L. Kholkin, I. K. Bdikin, V. V. Shvartsman, and N. A. Pertsev. *Nanotechnology*, 18:095502, 2007.

[85] R. Proksch. *arXiv preprint arXiv:1409.0133*, 2014.

[86] M. Molotskii. *J. Appl. Phys.*, 93:6234, 2003.

[87] F. Felten, G. A. Schneider, J. Muñoz Saldana, and S. V. Kalinin. *J. Appl. Phys.*, 96:563, 2004.

[88] D. A. Scrymgeour and V. Gopalan. *Phys. Rev. B*, 72:024103, 2005.

[89] A. N. Morozovska, E. A. Eliseev, S. L. Bravina, and S. V. Kalinin. *Phys. Rev. B*, 75:174109, 2007.

[90] K. Seal, S. Jesse, B. J. Rodriguez, A. P. Baddorf, and S. V. Kalinin. *Appl. Phys. Lett.*, 91:232904, 2007.

[91] C. Harnagea, M. Alexe, D. Hesse, and A. Pignolet. *Appl. Phys. Lett.*, 83:338, 2003.

[92] C. Harnagea, M. Alexe, D. Hesse, and A. Pignolet. *IEEE Trans. on Ultrasonics, Ferroelectrics and Frequency Control*, 53:2309, 2006.

[93] S. Jesse, S. Guo, A. Kumar, B. J. Rodriguez, R. Proksch, and S. V. Kalinin. *Nanotechnology*, 21:405703, 2010.

[94] R. Nath, Y.-C. Chu, N. A. Polomoff, R. Ramesh, and B. D. Huey. *Appl. Phys. Lett.*, 92:072905, 2008.

[95] I. K. Bdikin, V. V. Shvartsman, S.-H. Kim, J. Manuel Herrero, and A. L. Kholkin. Frequency-dependent electromechanical response in ferroelectric materials measured via piezoresponse force microscopy. In *MRS Proceedings*, volume 784, pages C11–3. Cambridge Univ Press, 2003.

[96] S. Jesse, A. P. Baddorf, and S. V. Kalinin. *Nanotechnology*, 17:1615, 2006.

[97] B. J. Rodriguez, C. Callahan, S. V. Kalinin, and R. Proksch. *Nanotechnology*, 18:475504, 2007.

[98] S. Jesse, S. V. Kalinin, R. Proksch, A. P. Baddorf, and B. J. Rodriguez. *Nanotechnology*, 18:435503, 2007.

[99] K. Romanyuk, S. Yu. Luchkin, M. Ivanov, A. Kalinin, and A. L. Kholkin. *Microsc. Microanal.*, 21:154, 2015.

[100] A. Gannepalli, D. G. Yablon, A. H. Tsou, and R. Proksch. *Nanotechnology*, 22:355705, 2011.

[101] C.-E. Cheng, H.-J. Liu, F. Dinelli, Y.-C. Chen, C.-S. Chang, F. S.-S. Chien, and Y.-H. Chu. *Sci. Rep.*, 5:809, 2015.

[102] N. Balke, S. Jesse, Y.-H. Chu, and S. V. Kalinin. *ACS Nano*, 6:5559, 2012.

[103] C. Harnagea, M. Vallières, C. P. Pfeffer, D. Wu, B. R. Olsen, A. Pignolet, F. Légaré, and A. Gruverman. *Biophys. J.*, 98:3070, 2010.

[104] J. E. Sader. *Rev. Sci. Instrum.*, 74:2438, 2003.

[105] C. Harnagea. Local piezoelectric response and domain structures in ferroelectric thin films investigated by voltage-modulated force microscopy, 2001. PhD thesis, Martin-Luther University Halle-Wittenberg.

[106] S. Jesse, A. P. Baddorf, and S. V. Kalinin. *Appl. Phys. Lett.*, 88:062908, 2006.

[107] Y. Kim, A. Kumar, O. Ovchinnikov, S. Jesse, H. Han, D. Pantel I. Vrejoiu, W. Lee, D. Hesse, M. Alexe, and S. V. Kalinin. *ACS Nano*, 6:491, 2012.

[108] R. Lüthi, H. Haefke, K.-P. Meyer, E. Meyer, L. Howald, and H.-J. Güntherodt. *J. Appl. Phys.*, 74:7461, 1993.

[109] T. Mitsui and J. Furuichi. *Phys. Rev.*, 90:193, 1953.

[110] A. K. Tagantsev, L. E. Cross, and J. Fousek. *Domains in Ferroic Crystals and Thin Films*. Springer, New York, USA, 2010.

[111] S. K. Streiffer, J. A. Eastman, D. D. Fong, Carol Thompson, A. Munkholm, M. V. Ramana Murty, O. Auciello, G. R. Bai, and G. B. Stephenson. *Phys. Rev. Lett.*, 89:067601, 2002.

[112] A. Schilling, D. Byrne, G. Catalan, K. G. Webber, Y. A. Genenko, G. S. Wu, J. F. Scott, and J. M. Gregg. *Nano Lett.*, 9:3359, 2009.

[113] B. J. Rodriguez, X. S. Gan, L. F. Liu, W. Lee, I. I. Naumov, A. M. Bratkovsky, D. Hesse, and M. Alexe. *Nano Lett.*, 9:1127, 2009.

[114] C. Lichtensteiger, S. Fernandez-Peña, C. Weymann, P. Zubko, and J.-M. Triscone. *Nano Lett.*, 14:4205, 2014.

[115] B. J. Rodriguez, S. Choudhury, Y. H. Chu, A. Bhattacharya, S. Jesse, K. Seal, A. P. Baddorf, R. Ramesh, L.-Q. Chen, and S. V. Kalinin. *Adv. Funct. Mat.*, 19:2053, 2009.

[116] B. J. Rodriguez, S. Jesse, A. P. Baddorf, T. Zhao, Y. H. Chu, R. Ramesh, E. A. Eliseev, A. N. Morozovska, and S. V. Kalinin. *Nanotechnology*, 18:405701, 2007.

[117] Y.-H. Hsieh, E. Strelcov, J.-M. Liou, C.-Y. Shen, Y.-C. Chen, S. V. Kalinin, and Y.-H. Chu. *ACS Nano*, 7:8627, 2013.

[118] J. Seidel, L. W. Martin, Q. He, Q. Zhan, Y.-H. Chu, A. Rother, M. E. Hawkridge, P. Maksymovych, P. Yu, M. Gajek, N. Balke, S. V. Kalinin, S. Gemming, F. Want, G. Catalan, J. F. Scott, N. A. Spaldin, J. Orenstein, and R. Ramesh. *Nature Mater.*, 8:229, 2009.

[119] S. Y. Yang, J. Seidel, S. J. Byrnes, P. Shafer, C.-H Yang, M. D. Rossell, P. Yu, Y.-H. Chu, J. F. Scott, J. W. Ager III, L. W. Martin, and R. Ramesh. *Nature Nanotech.*, 5:143, 2010.

[120] A. Bhatnagar, A. R. Chaudhuri, Y. H. Kim, D. Hesse, and M. Alexe. *Nature Comm.*, 4:2835, 2013.

[121] G. Catalan, J. Seidel, R. Ramesh, and J. F. Scott. *Rev. Mod. Phys.*, 84:119, 2012.

[122] R. K. Vasudevan, W. Wu, J. R. Guest, A. P. Baddorf, A. N. Morozovska, E. E. Eliseev, N. Balke, V. Nagarajan, P. Maksymovych, and S. V. Kalinin. *Adv. Funct. Mat.*, 23:2592, 2013.

[123] C. S. Ganpule, V. Nagarajan, B. K. Hill, A. L. Roytburd, E. D. Williams, S. P. Alpay, A. Roelofs, R. Waser, and L. M. Eng. *J. Appl. Phys.*, 91:1477, 2002.

[124] M. Park, S. Hong, J. A. Klug, M. J. Bedzyk, O. Auciello, K. No, and A. Petford-Long. *Appl. Phys. Lett.*, 97:112907, 2010.

[125] R. Nath, S. Hong, J. A. Klug, A. Imre, M. J. Bedzyk, R. S. Katiyar, and O. Auciello. *Appl. Phys. Lett.*, 96:163101, 2010.

[126] T. Jungk, Á. Hoffman, and E. Soergel. *Appl. Phys. Lett.*, 89:042901, 2006.

[127] J. Guyonnet, H. Béa, F. Guy, S. Gariglio, S. Fusil, K. Bouzehouane, J.-M. Triscone, and P. Paruch. *Appl. Phys. Lett.*, 95:132902, 2009.

[128] J. Guyonnet, H. Béa, and P. Paruch. *J. Appl. Phys.*, 108:042002, 2010.

[129] W. Eerenstein, N. D. Mathur, and J. F. Scott. *Nature*, 442:759, 2006.

[130] M. Fiebig. *J. Phys. D: Appl. Phys*, 38:R123, 2005.

[131] G. Catalan, H. Béa, S. Fusil, M. Bibes, P. Paruch, A. Barthélémy, and J. F. Scott. *Phys. Rev. Lett.*, 100:027602, 2008.

[132] S. Farokhipoor and B. Noheda. *J. Appl. Phys.*, 112:052003, 2012.

[133] N. Balke, S. Choudhury, S. Jesse, M. Huijben, Y. H. Chu, A. P. Baddorf, L. Q. Chen, R. Ramesh, and S. V. Kalinin. *Nature Nanotech.*, 4:868, 2009.

[134] H. Béa, B. Ziegler, M. Bibes, A. Barthélémy, and P. Paruch. *J. Phys.: Condens. Matter*, 23:142201, 2011.

[135] R. K. Vasudevan, Y. Liu, J. Li, W.-I. Liang, A. Kumar, S. Jesse, Y.-C. Chen, Y.-H. Chu, V. Nagarajan, and S. V. Kalinin. *Nano Lett.*, 11:3346, 2011.

[136] Y.-C. Chen, Q. He, F.-N. Chu, Y.-C. Huang, J.-W. Chen, W.-I Liang, R. K. Vasudevan, V. Nagarajan, E. Arenholz, S. V. Kalinin, and Y.-H. Chu. *Adv. Mat.*, 24:3070, 2012.

[137] G. Catalan and J. F. Scott. *Adv. Mat.*, 21:2463, 2009.

[138] G. M. De Luca, D. Preziosi, F. Chiarella, R. Di Capua, S. Gariglio, S. Lettieri, and M. Salluzo. *Appl. Phys. Lett.*, 103:062902, 2013.

[139] S. Mukherjee, A. Roy, S. Auluck, R. Prasad, R. Gupta, and A. Garg. *Phys. Rev. Lett.*, 111:087601, 2013.

[140] R. Zhang, C. Chen, M. Duan, L. Niu, and K. Jin. *J. Cryst. Growth*, 390:56–60, 2014.

[141] W. Wang, J. Zhao, W. Wang, Z. Gai, N. Balke, M. Chi, H. N. Lee, W. Tian, L. Zhu, X. Cheng, D. J. Keavney, J. Yi, T. Z. Ward, P. C. Snijders, H. M. Christen, W. Wu, J. Shen, and X. Xu. *Phys. Rev. Lett.*, 110:237601, 2013.

[142] L. Keeney, T. Maity, M. Schmidt, A. Amann, N. Deepak, N. Petkov, S. Roy, M. E. Pemble, and R. W. Whatmore. *J. Am. Ceram. Soc.*, 96:2339, 2013.

[143] I. Levin, J. Li, J. Slutsker, and A. L. Roytburd. *Adv. Mat.*, 18:2044, 2006.

[144] F. Zavaliche, T. Zhao, H. Zheng, F. Straub, M. P. Cruz, P.-L. Yang, D. Hao, and R. Ramesh. *Nano Lett.*, 7:1586, 2007.

[145] S. Geprägs, A. Brandlmaier, M. Opel, R. Gross, and S. T. B. Goennenwein. *Appl. Phys. Lett.*, 96:142509, 2010.

[146] V. Skumryev, V. Laukhin, I. Fina, X. Martí, F. Sánchez, M. Gospodinov, and J. Fontcuberta. *Phys. Rev. Lett.*, 106:057206, 2011.

[147] C. A. F. Vaz. *J. Phys.: Condens. Matter*, 24:333201, 2012.

[148] D. M. Evans, A. Schilling, A. Kumar, D. Sanchez, N. Ortega, M. Arredondo, R. S. Katiyar, J. M. Gregg, and J. F. Scott. *Nature Comm.*, 4:1534, 2012.

[149] H. Trivedi, V. V. Shvartsman, D. C. Lupascu, M. S. A. Medeiros, R. C. Pullar, A. L. Kholkin, P. Zelenovskiy, A. Sosnovskikh, and V. Ya. Shur. *Nanoscale*, 7:4489, 2015.

[150] S. Jesse, B. J. Rodriguez, S Choudhury, A. P. Baddorf, I. Vrejoiu, D. Hesse, M. Alexe, E. A. Eliseev, A. N. Morozovska, J. Zhang, L.-Q. Chen, and S. V. Kalinin. *Nature Mater.*, 7:209, 2008.

[151] P. Bintachitt, S. Jesse, D. Damjanovic, Y.Han, I. M. Reaney, S. Trolier-McKinstry, and S. V. Kalinin. *Proc. Nat. Acad. Sci.*, 107:7219, 2010.

[152] O. Ovchinnikov, S. Jesse, S. Guo, K. Seal, P. Bintachitt, I. Fujii, S. Trolier-McKinstry, and S. V. Kalinin. *Appl. Phys. Lett.*, 96:112906, 2010.

[153] O. Ovchinnikov, S. Jesse, S. Guo, K. Seal, P. Bintachitt, I. Fujii, S. Trolier-McKinstry, and S. V. Kalinin. *J. Appl. Phys.*, 110:044109, 2011.

[154] R. K. Vasudevan, Y. Matsumoto, X. C., A. Imai, S. Maruyama, H.L. Xin, M.B. Okatan, S. Jesse, S.V. Kalinin, and V. Nagarajan. *Nature Comm.*, 5:4971, 2014.

[155] A. N. Morozovska, E. A. Eliseev, Y. Li, S. V. Svechnikov, P. Maksymovych, V. Y. Shur, V. Gopalan, L.-Q. Chen, and S. V. Kalinin. *Phys. Rev. B*, 80:214110, 2009.

[156] C. Blaser and P. Paruch. *Appl. Phys. Lett.*, 101:142906, 2012.

[157] A. Brugère, S. Gidon, and B. Gautier. *J. Appl. Phys.*, 110:052016, 2011.

[158] C. Blaser and P. Paruch. *Appl. Phys. Lett.*, 104:092908, 2014.

[159] B. J. Rodriguez, S. Jesse, A. P. Baddorf, S.-H. Kim, and S. V. Kalinin. *Phys. Rev. Lett.*, 98:247603, 2007.

[160] O. Auciello, A. Gruverman, and H. Tokumoto. *Integr. Ferroelectrics*, 15:107, 1997.

[161] A. L. Kholkin, Ch. Wütchrich, D. V. Taylor, and N. Setter. *Rev. Sci. Instrum.*, 67:1935, 2001.

[162] P. Bintachitt, S. Trolier-McKinstry, K. Seal, S. Jesse, and S. V. Kalinin. *Appl. Phys. Lett.*, 84:042906, 2009.

[163] A. Gruverman. *Appl. Phys. Lett.*, 75:1452, 1999.

[164] H. Fujisawa, T. Yagi, M. Shimizu, and H. Niu. *Ferroelectrics*, 269:21, 2002.

[165] D. J. Kim, J. Y. Jo, T. H. Kim, S. M. Yang, B. Chen, Y. S. Kim, and T. W. Noh. *Appl. Phys. Lett.*, 91:132903, 2007.

[166] S. V. Kalinin, B. J. Rodriguez, S.-H. Kim, S.-K. Hong, and A. Gruverman E. A. Eliseev. *Appl. Phys. Lett.*, 92:152906, 2008.

[167] A. Gruverman, B. J. Rodriguez, C. Dehoff, J. D. Waldrep, A. I. Kingon, and R. J. Nemanich. *Appl. Phys. Lett.*, 87:082902, 2005.

[168] A. Gruverman, D. Wu, and J. F. Scott. *Phys. Rev. Lett.*, 100:097601, 2008.

[169] D. J. Kim, J. Y. Jo, Y. S. Kim, and T. K. Song. *J. Phys. D: Appl. Phys*, 43:395403, 2010.

[170] S. M. Yang, J. Y. Jo, T. H. Kim, J.-G. Yoon, K. Song, H. N. Lee, Z. Marton, S. Park, Y. Jo, and T. W. Noh. *Phys. Rev. B*, 82:174125, 2010.

[171] T. Tybell, P. Paruch, T. Giamarchi, and J.-M. Triscone. *Phys. Rev. Lett.*, 89:097601, 2002.

[172] Y. Kim, H. Han, W. Lee, S. Baik, D. Hesse, and M. Alexe. *Nano Lett.*, 10:1266, 2010.

[173] C.-L. Jia, K. W. Urban, M. Alexe, D. Hesse, and I. Vrejoiu. *Science*, 331:1420, 2011.

[174] P. Paruch, A. B. Kolton, X. Hong, C. H. Ahn, and T. Giamarchi. *Phys. Rev. B*, 85:214115, 2012.

[175] J. Woo, S. Hong, N. Setter, H. Shin, J.-U. Jeon, Y.E. Pak, and K. No. *J. Vac. Sci. Tech. B*, 19:818, 2001.

[176] P. Paruch, T. Tybell, and J.-M. Triscone. *Appl. Phys. Lett.*, 79:530, 2001.

[177] X. R. Huang, X. B. Hu, S. S. Jiang, and D. Feng. *Phys. Rev. B*, 55:5534, 1997.

[178] B. Meyer and D. Vanderbilt. *Phys. Rev. B*, 65:104111, 2002.

[179] D. Lee, R. K. Behera, P. Wu, H. Xu, Y. L. Li, S. B. Sinnott, W. R. Phillpot, L. Q. Chen, and V. Gopalan. *Phys. Rev. B*, 80:060102, 2009.

[180] Y. L. Li, S. Y. Hu, Z. K. Liu, and L. Q. Chen. *Appl. Phys. Lett.*, 78:3878, 2001.

[181] T. Giamarchi, A. B. Kolton, and A. Rosso. Dynamics of disordered elastic systems. In M. C. Miguel and J. M. Rubi, editors, *Jamming, Yielding and Irreversible deformation in condensed matter*, pages 91–108, Berlin/Heidelberg, 2006. Springer.

[182] B. B. Mandelbrot, D. E. Passoja, and A. J. Paullay. *Nature*, 308:721, 1984.

[183] M.A. Rubio, C.A. Edwards, A. Dougherty, and J.P. Gollub. *Phys. Rev. Lett.*, 63:1685, 1989.

[184] M. Myllys, J. Maunuksela, M. J. Alava, T. Ala-Nissila, and J. Timonen. *Phys. Rev. Lett.*, 84:1946, 2000.

[185] J. A. Bonachela, C. D. Nadell, J. B. Xavier, and S. A. Levin. *J. Stat. Phys.*, 144:303, 2011.

[186] T. Speck and R. L. C. Vink. *Phys. Rev. E*, 86:031923, 2012.

[187] P. Paruch, T. Giamarchi, T. Tybell, and J.-M. Triscone. *J. Appl. Phys.*, 100:051608, 2006.

[188] J. Guyonnet, S. Bustingorry, C. Blaser, E. E. Ferrero, I. Gaponenko, J. Karthik, L. W. Martin, and P. Paruch. Manuscript in preparation.

[189] P. Paruch and J. Guyonnet. *C. R. Physique*, 14:667, 2013.

[190] N. A. Pertsev, D. A. Kiselev, I. K. Bdikin, M. Kosec, and A. L. Kholkin. *J. Appl. Phys.*, 110:052001, 2011.

[191] N. A. Pertsev, A. Petraru, H. Kohlstedt, R. Waser, I. K. Bdikin, D. Kiselev, and A. L. Kholkin. *Nanotech.*, 19:375703, 2008.

[192] A. N. Kolmogorov. *Izv. Akad. Nauk. Ser. Math.*, 3:355, 1937.

[193] M. Avrami. *J. Chem. Phys.*, 8:212, 1940.

[194] Y. Ishibashi and Y. Takagi. *J. Phys. Soc. Jpn.*, 31:506, 1971.

[195] T. D. Usher, C. P. Poole, and H. A. Farach. *Ferroelectrics*, 120:201, 1991.

[196] W. Li and M. Alexe. *Appl. Phys. Lett.*, 91:262903, 2007.

[197] A. K. Tagantsev, I. Stolichnov, and N. Setter. *Phys. Rev. B*, 66:214109, 2002.

[198] V. Ya. Shur, E. Rumyantsev, and S. Makarov. *J. Appl. Phys.*, 84:445, 1998.

[199] A. L. Kholkin, A. N. Morozovska, D. Kiselev, I. K. Bdikin, B. J. Rodriguez, P. Wu, A. Bokov, Z.-G. Ye, B. Dkhil, L.-Q. Chen, M. Kosec, and S. V. Kalinin. *Adv. Funct. Mat.*, 21:1977, 2011.

[200] A. V. Ievlev, A. N. Morozovska, V. Ya. Shur, and S. V. Kalinin. *Appl. Phys. Lett.*, 104:092908, 2014.

[201] J. Guyonnet, I. Gaponenko, S. Gariglio, and P. Paruch. *Adv. Mat.*, 23:5377, 2011.

[202] C. R. Wrinkler, A. R. Damodaran, J. Karthik, L. W. Martin, and M. L. Taheri. *Micron*, 43:1121, 2012.

[203] P. Gupta, H. Jain, D. B. Williams, S. V. Kalinin, J. Shin, S. Jesse, and A. P. Baddorf. *Appl. Phys. Lett.*, 87:172903, 2005.

[204] T. L. Burnett, P. M. Weaver, J. F. Blackburn, M. Stewart, and M. G. Cain. *J. Appl. Phys.*, 108:042001, 2010.

[205] N. Barrett, J. E. Rault, J. L Wang, C. Mathieu, A. Locatelli, T. O Mentes, M. A. Niño, S. Fusil, M. Bibes, A. Barthélémy, D. Sando, W. Ren, S. Prosandeev, L. Bellaiche, B. Vilquin, A. Petraru, I. P. Krug, and C. M. Schneider. *J. Appl. Phys.*, 113:187217, 2013.

[206] W.-C. Yang, B. J. Rodriguez, A. Gruverman, and R. J. Nemanich. *Appl. Phys. Lett.*, 85:2316, 2004.

[207] J. E. Rault, T. O. Mentes, A. Locatelli, and N. Barrett. *Scientific Reports*, 4:6792, 2014.

[208] J. R. Whyte, R. G. P. McQuaid, P. Sharma, C. Canalias, J. F. Scott, A. Gruverman, and J. M. Gregg. *Adv. Mat.*, 26:293, 2014.

[209] L. J. McGilly, P. Yudin, L. Feigl, A. K. Tagantsev, and N. Setter. *Nature Nanotech.*, 10:145, 2015.

[210] B. J. Rodriguez, A. Gruverman, and R. J. Nemanich. Nanoscale characterization of electronic and electrical properties of III-nitrides by scanning probe microscopy. In S. V. Kalinin and A. Gruverman, editors, *Scanning Probe Microscopy*, pages 690–714. Springer, New York, USA, 2007.

[211] J. A. Christman, R. R. Woolcott, A. I. Kingon, and R. J. Nemanich. *Appl. Phys. Lett.*, 73:3851, 1998.

[212] A. Gruverman, O. Auciello, and H. Tokumoto. *J. Vac. Sci. Technol., B*, 14:602, 1996.

[213] R. F. Davis. *Proc. IEEE*, 79:702, 1991.

[214] O. Ambacher, J. Smart, J. R. Shealy, N. G. Weimann, K. Chu, M. Murphy, W. J. Schaff, L. F. Eastman, R. Dimitrov, L. Wittmer, M. Stutzmann, W. Rieger, and J. Hilsenbeck. *J. Appl. Phys.*, 85:3222, 1999.

[215] J. Song, J. Zhou, and Z. L. Wang. *Nano Lett.*, 6:1656, 2006.

[216] Z. L. Wang. *Appl. Phys. A*, 88:7, 2007.

[217] M.-A. Dubois and P. Muralt. *Sens. Actuators A: Phys.*, 77:106, 1999.

[218] X. Xu, A. Potié, R. Songmuang, J. W. Lee, B. Bercu, T. Baron, B. Salem, and L. Montès. *Nanotechnology*, 22:105704, 2011.

[219] A. Gruverman, W. Cao, S. Bhaskar, and S. K. Dey. *Appl. Phys. Lett.*, 84:5153, 2004.

[220] I. Stolichnov, L. Malin, P. Muralt, and N. Setter. *Appl. Phys. Lett.*, 88:043512, 2006.

[221] A. Ohtomo and H. Y. Hwang. *Nature*, 427:423, 2004.

[222] C. W. Bark, P. Sharma, Y. Wang, S. H. Baek, S. Lee, S. Ryu, C. M. Folkman, T. R. Paudel, A. Kumar, S. V. Kalinin, A. Sokolov, E. Y. Tsymbal, M. S. Rzchowski, A. Gruverman, and C. B. Eom. *Nano Lett.*, 12:1765, 2012.

[223] B. J. Rodriguez, A. Gruverman, A. I. Kingon, R. J. Nemanich, and O. Ambacher. *Appl. Phys. Lett.*, 80:4166, 2002.

[224] C. K. Lee, F. Placido, S. Cochran, and K. J. Kirk. Growth of sputtered aln thin film on glass in room temperature. In *Ultrasonics Symposium, 2002. Proceedings. 2002 IEEE*, volume 2, pages 1119–1122, Munich, 2002. IEEE.

[225] M. Akiyama, T. Kamohara, N. Ueno, M. Sakamoto, K. Kano, A. Teshigahara, and N. Kawahara. *Appl. Phys. Lett.*, 90:151910, 2007.

[226] A. Artieda, C. Sandu, and P. Muralt. *J. Vac. Sci. Technol., A*, 28:390, 2010.

[227] B. J. Rodriguez, A. Gruverman, A. I. Kingon, and R. J. Nemanich. *J. Cryst. Growth*, 246:252, 2002.

[228] M. D. Brubaker, I. Levin, A. V. Davydov, D. M. Rourke, N. A. Sanford, V. M. Bright, and K. A. Bertness. *J. Appl. Phys.*, 110:053506, 2011.

[229] R. Dalmau, R. Schlesser, B. J. Rodriguez, R. J. Nemanich, and Z. Sitar. *J. Cryst. Growth*, 281:68–74, 2005.

[230] K. Tonisch, V. Cimalla, C. Foerster, H. Romanus, O. Ambacher, and D. Dontsov. *Sens. Actuators A: Phys.*, 132:658, 2006.

[231] K. Tonisch, V. Cimalla, C. Foerster, D. Dontsov, and O. Ambacher. *Phys. Status Solidi C*, 3:2274, 2006.

[232] M. Minary-Jolandan, R. A. Bernal, I. Kuljanishvili, V. Parpoil, and H. D. Espinosa. *Nano Lett.*, 12:970, 2012.

[233] T. Stoica, R. Calarco, R. Meijers, and H. Lüth. *Appl. Surf. Sci.*, 253:4300, 2007.

[234] A. Zukauskaite, G. Wingqvist, J. Palisaitis, J. Jensen, P. O. Persson, R. Matloub, P. Muralt, Y. Kim, J. Birch, and L. Hultman. *J. Appl. Phys.*, 111:093527, 2012.

[235] S. N. Babu, S.-G. Min, A. Yourdkhani, G. Caruntu, and L. Malkinski. *J. Appl. Phys.*, 111:07C720, 2012.

[236] M. Minary-Jolandan, R. A. Bernal, and H. D. Espinosa. *MRS Comm.*, 1:45, 2011.

[237] M.-H. Zhao, Z.-L. Wang, and S. X. Mao. *Nano Lett.*, 4:587, 2004.

[238] K. Momeni, A. Asthana, A. Prasad, Y. K. Yap, and R. Shahbazian-Yassar. *Appl. Phys. A*, 109:95, 2012.

[239] H. J. Fan, W. Lee, R. Hauschild, M. Alexe, G. Le Rhun, R. Scholz, A. Dadgar, K. Nielsch, H. Kalt, A. Krost, M. Zacharias, and U. Gösele. *Small*, 2:561, 2006.

[240] D. A. Scrymgeour, T. L. Sounart, N. C. Simmons, and J. W. P. Hsu. *J. Appl. Phys.*, 101:014316, 2007.

[241] D. A. Scrymgeour and J. W. P. Hsu. *Nano Lett.*, 8:2204, 2008.

[242] L. P. Schuler, N. Valanoor, P. Miller, I. Guy, R. J. Reeves, and M. M. Alkaisi. *J. Electron. Mater.*, 36:507, 2007.

[243] C. P. Li and B. H. Yang. *J. Electron. Mater.*, 40:253, 2011.

[244] K.-M. Zhang, Y.-P. Zhao, F.-Q. He, and D.-Q. Liu. *Chinese J. Chem. Phys.*, 20:721, 2007.

[245] J. S. Park, J. H. Chang, T. Minegishi, H. J. Lee, S. H. Park, I. H. Im, T. Hanada, S. K. Hong, M. W. Cho, and T. Yao. *J. Electron. Mater.*, 37:736, 2008.

[246] J. S. Park, T. Minegishi, S. H. Lee, I. H. Im, S. H. Park, T. Goto, M. W. Cho, T. Yao, S. K. Hong, J. W. Lee, J. Y. Lee, S. Ahn, H. Jeon, W. Lee, M. N. Jung, and J. H. Chang. *J. Vac. Sci. Technol. B*, 27:1658, 2009.

[247] I. K. Bdikin, J. Gracio, R. Ayouchi, R. Schwarz, and A. L. Kholkin. *Nanotech.*, 21:235703, 2010.

[248] Y. C. Yang, C. Song, X. H. Wang, F. Zeng, and F. Pan. *J. Appl. Phys.*, 103:074107, 2008.

[249] Y. C. Yang, C. Song, X. H. Wang, F. Zeng, and F. Pan. *Appl. Phys. Lett.*, 92:012907, 2008.

[250] Y. Q. Chen, X. J. Zheng, and X. Feng. *Nanotechnology*, 21:055708, 2010.

[251] F. Pan, J.-T. Luo, Y.-C. Yang, X.-B. Wang, and F. Zeng. *Sci. China Technol. Sci.*, 55:421, 2012.

[252] W. L. Ong, H. Huang, J. Xiao, K. Zeng, and G. W. Ho. *Nanoscale*, 6:1680, 2014.

[253] A. N. Morozovska, S. V. Svechnikov, E. A. Eliseev, S. Jesse, B. J. Rodriguez, and S. V. Kalinin. *J. Appl. Phys.*, 102:114108, 2007.

[254] Y. Kim, S. J. Kelly, A. N. Morozovska, E. K. Rahani, E. Strelcov, E. A. Eliseev, S. Jesse, M. D. Biegalski, N. Balke, N. Benedek, D. Strukov, J. Aarts, I. Hwang, S. Oh, J. S. Choi, T. Choi, B. H. Park, V. B. Shenoy, P. Maksymovych, and S. V. Kalinin. *Nano Lett.*, 13:4068, 2013.

[255] C. Liu, S. Hu, and S. Shen. *Smart Mater. Struct.*, 21:115024, 2012.

[256] B. J. Rodriguez, S. Jesse, J. Kim, S. Ducharme, and S. V. Kalinin. *Appl. Phys. Lett.*, 92:232903, 2008.

[257] R. K. Vasudevan, S. Jesse, Y. Kim, A. Kumar, and S. V. Kalinin. *MRS Comm.*, 2:61, 2012.

[258] I. L. Guy, S. Muensit, and E. M. Goldys. *Appl. Phys. Lett.*, 75:3641, 1999.

[259] A. N. Morozovska, E. A. Eliseev, N. Balke, and S. V. Kalinin. *J. Appl. Phys.*, 108:053712, 2010.

[260] A. Kumar, F. Ciucci, A. N. Morozovska, S. V. Kalinin, and S. Jesse. *Nat. Chem.*, 3:707, 2011.

[261] E. J. Miller, D. M. Schaadt, E. T. Yu, C. Poblenz, C. Elsass, and J. S. Speck. *J. Appl. Phys.*, 91:9821, 2002.

[262] V. S. Bystrov, I. K. Bdikin, A. Heredia, R. C. Pullar, E. D. Mishina, A. S. Sigov, and A. L. Kholkin. Piezoelectricity and ferroelectricity in biomaterials: from proteins to self-assembled peptide nanotubes. In G. Ciofiani and A. Menciassi, editors, *Piezoelectric Nanomaterials for Biomedical Applications*, pages 187–211. Springer, New York, USA, 2012.

[263] R. M. Green. *Am. J. Med. Sci.*, 227:231, 1954.

[264] H. Athenstaedt. *Ann. N. Y. Acad. Sci.*, 238:68, 1974.

[265] V. S. Bystrov. *Ferroelectrics Lett.*, 23:87, 1997.

[266] E. Fukada and I. Yasuda. *J. Phys. Soc. Jpn.*, 12:1158, 1957.

[267] E. Fukada and I. Yasuda. *Jpn. J. Appl. Phys.*, 3:117, 1964.

[268] A. A. Marino and B. D. Gross. *Arch. Oral Biol.*, 34:507, 1989.

[269] E. Fukada. *J. Phys. Soc. Jpn.*, 10:149, 1955.

[270] S. V. Kalinin, B. J Rodriguez, J. Shin, S. Jesse, V. Grichko, T. Thundat, A. P. Baddorf, and A. Gruverman. *Ultramicroscopy*, 106:334, 2006.

[271] T. Li and K. Zeng. *Acta Mater.*, 59:3667, 2011.

[272] Majid Minary-Jolandan and Min-Feng Yu. *Nanotechnology*, 20:085706, 2009.

[273] V. V. Lemanov, S. N. Popov, and G. A. Pankova. *Phys. Solid State*, 44:1929, 2002.

[274] M. Wojtás, A. Gagor, and A. L. Kholkin. *J. Mol. Struct.*, 1075:213, 2014.

[275] A. T. Todorov, A. G. Petrov, and J. H. Fendler. *J. Phys. Chem.*, 98:3076, 1994.

[276] Y. Liu, Y. Zhang, M.-J. Chow, Q. N. Chen, and J. Li. *Phys. Rev. Lett.*, 108:078103, 2012.

[277] B. Y. Lee, J. Zhang, C. Zueger, W. Chung, S. Y. Yoo, E. Wang, J. Meyer, R. Ramesh, and S. Lee. *Nature Nanotech.*, 7:351, 2012.

[278] C. Halperin, S. Mutchnik, A. Agronin, M. Molotskii, P. Urenski, M. Salai, and G. Rosenman. *Nano Lett.*, 4:1253, 2004.

[279] G. B. Reinish and A. S. Nowick. *Nature*, 253:626, 1975.

[280] S. Ghosh, B. Z. Mei, V. Lubkin, J. I. Scheinbeim, B. A. Newman, P. Kramer, G. Bennett, and N. Feit. *J. Biomed. Mater. Res.*, 39:453, 1998.

[281] A. C. Jayasuriya, S. Ghosh, J. I. Scheinbeim, V. Lubkin, G. Bennett, and P. Kramer. *Biosens. Bioelectron.*, 18:381, 2003.

[282] A. C. Jayasuriya, J. I. Scheinbeim, V. Lubkin, G. Bennett, and P. Kramer. *J. Biomed. Mater. Res., Part A*, 66:260, 2003.

[283] K. Uchino. *Piezoelectric actuators and ultrasonic motors*, volume 1. Springer, New York, USA, 1997.

[284] T. W. Kelley, P. F. Baude, C. Gerlach, D. E. Ender, D. Muyres, M. A. Haase, D. E. Vogel, and S. D. Theiss. *Chem. Mater.*, 16:4413, 2004.

[285] D. A. Bonnell. *Science*, 339:401, 2013.

[286] D.-W. Fu, H.-L. Cai, Y. Liu, Q. Ye, W. Zhang, Y. Zhang, X.-Y. Chen, G. Giovannetti, M. Capone, J. Li, and R.-G. Xiong. *Science*, 339:425, 2013.

[287] S. Horiuchi, Y. Tokunaga, G. Giovannetti, S. Picozzi, H. Itoh, R. Shimano, R. Kumai, and Y. Tokura. *Nature*, 463:789, 2010.

[288] S. Horiuchi, F. Kagawa, K. Hatahara, K. Kobayashi, R. Kumai, Y. Murakami, and Y. Tokura. *Nature Comm.*, 3:1308, 2012.

[289] B. J. Rodriguez, S. Jesse, S. V. Kalinin, J. Kim, S. Ducharme, and V. M. Fridkin. *Appl. Phys. Lett.*, 90:122904, 2007.

[290] P. Sharma, D. Wu, S. Poddar, T. J. Reece, S. Ducharme, and A. Gruverman. *J. Appl. Phys.*, 110:052010, 2011.

[291] I. K. Bdikin, V. Bystrov, S. Kopyl, R. P. G. Lopes, I. Delgadillo, J. Gracio, E. Mishina, A. Sigov, and A. L. Kholkin. *Appl. Phys. Lett.*, 100:043702, 2012.

[292] N. Kol, L. Adler-Abramovich, D. Barlam, R. Z. Shneck, E. Gazit, and I. Rousso. *Nano Lett.*, 5:1343, 2005.

[293] E. Gazit. *Chem. Soc. Rev.*, 36:1263, 2007.

[294] M. Reches and E. Gazit. *Science*, 300:625, 2003.

[295] Z. Hu, M. Tian, B. Nysten, and A. M. Jonas. *Nature Mater.*, 8:62, 2008.

[296] K. N. Unni, R. de Bettignies, S. Dabos-Seignon, and J.-M. Nunzi. *Appl. Phys. Lett.*, 85:1823, 2004.

[297] T. Li and K. Zeng. *J. Appl. Phys.*, 113:187202, 2013.

[298] A. Heredia, V. Meunier, I. K. Bdikin, J. Gracio, N. Balke, S. Jesse, A. Tselev, P. K. Agarwal, B. G. Sumpter, S. V. Kalinin, and A. L. Kholkin. *Adv. Funct. Mat.*, 22:2996, 2012.

[299] B. Chen and H. Gao. *Phys. Online J.*, 5:19, 2012.

[300] T. Niori, T. Sekine, J. Watanabe, T. Furukawa, and H. Takezoe. *J. Mater. Chem.*, 6:1231, 1996.

[301] S. Abeygunaratne, A. Jákli, G. Milkereit, H. Sawade, and V. Vill. *Phys. Rev. E*, 69:021703, 2004.

[302] Y. Liu, Y. Wang, M.-J. Chow, N. Q. Chen, F. Ma, Y. Zhang, and J. Li. *Phys. Rev. Lett.*, 110:168101, 2013.

[303] E. Konova, S. Baydanoff, M. Atanasova, and A. Velkova. *Exp. Gerontol.*, 39:249, 2004.

[304] H. Tomizawa, M. Yamazaki, K. Kunika, M. Itakura, and K. Yamashita. *Diabetes Res.Clin. Pr.*, 19:1, 1993.

[305] R. V. Gaynutdinov, O. A. Lysova, A. L. Tolstikhina, A. L. Kholkin, V. M. Fridkin, and S. Ducharme. *Appl. Phys. Lett.*, 95:023303, 2009.

[306] Y. Luo, P. Göring, M. Steinhart, M. Geuß, and K. Rademann. *Annual report des MPI für Mikrostrukturphysik Halle*, page 42, 2004.

[307] H. S. Nalwa. *Ferroelectric Polymers: Chemistry: Physics, and Applications*, volume 28. CRC Press, Boca Raton, Florida, 1995.

[308] Y. Kim, W. Kim, H. Choi, S. Hong, H. Ko, H. Lee, and K. No. *Appl. Phys. Lett.*, 96:012908, 2010.

[309] P. Sharma, T. J. Reece, S. Ducharme, and A. Gruverman. *Nano Lett.*, 11:1970, 2011.

[310] Z. Xiao, S. Poddar, S. Ducharme, and X. Hong. *Appl. Phys. Lett.*, 103:112903, 2013.

[311] D. A. Cisneros, J. Friedrichs, A. Taubenberger, C. M. Franz, and D. J. Müller. *Small*, 3:956, 2007.

[312] R. Gruschwitz, J. Friedrichs, M. Valtink, C. M. Franz, D. J. Müller, R. H. W. Funk, and K. Engelmann. *Invest. Ophthalmol. Vis. Sci.*, 51:6303, 2010.

[313] M. P. Lutolf and J. A. Hubbell. *Nat. Biotechnol.*, 23:47, 2005.

[314] H.-I. Chang and Y. Wang. Cell responses to surface and architecture of tissue engineering scaffolds. In D. Eberli, editor, *Regenerative Medicine and Tissue Engineering – Cells and Biomaterials*, pages 569–588. InTech, Rijeka, 2011.

[315] M. C. Prewitz, F. P. Seib, M. von Bonin, J. Friedrichs, A. Stissel, C. Niehage, K. Müller, K. Anastassiadis, C. Waskow, B. Hoflack, M. Bornhäuser, and C. Werner. *Nat. Methods*, 10:788, 2013.

[316] R. D. Rabbitt, H. E. Ayliffe, D. Christensen, K. Pamarthy, C. Durney, S. Clifford, and W. E. Brownell. *Biophys. J.*, 88:2257, 2005.

[317] Y. Kim, E. Strelcov, I. R. Hwang, T. Choi, B. H. Park, S. Jesse, and S. V. Kalinin. *Sci. Rep.*, 3:2924, 2013.

[318] Y. Kim, A. Kumar, A. Tselev, I. I. Kravchenko, H. Han, I. Vrejoiu, W. Lee, D. Hesse, M. Alexe, S. V. Kalinin, and S. Jesse. *ACS Nano*, 5:9104, 2011.

[319] A. N. Morozovska, E. A. Eliseev, A. K. Tagantsev, S. L. Bravina, L.-Q. Chen, and S. V. Kalinin. *Phys. Rev. B*, 83:195313, 2011.

[320] A. Tselev, A. N. Morozovska, A. Udod, E. A. Eliseev, and S. V. Kalinin. *Nanotechnology*, 25:445701, 2014.

[321] S. V. Kalinin, A. Borisevich, and D. Fong. *ACS Nano*, 6:10423, 2012.

[322] E. Strelcov, Y. Kim, S. Jesse, Y. Cao, I. N. Ivanov, I. I. Kravchenko, Ch.-H. Wang, Y.-C. Teng, L.-Q. Chen, Y. H. Chu, and S. V. Kalinin. *Nano Lett.*, 13:3455, 2013.

[323] R. Proksch. *J. Appl. Phys.*, 116:066804, 2014.

[324] J. S. Sekhon, L. Aggarwal, and G. Sheet. *Appl. Phys. Lett.*, 104:162908, 2014.

[325] J. F. Scott. *J. Phys.: Condens. Matter*, 20:021001, 2008.

[326] H. Miao, C. Tan, X. Zhou, X. Wei, and F. Li. *Europhys. Lett.*, 108:27010, 2014.

[327] S. Jyotsna, A. Arora, J. S. Sekhon, and G. Sheet. *J. Appl. Phys.*, 116:104903, 2014.

[328] Y. Kim, A. N. Morozovska, A. Kumar, S. Jesse, E. A. Eliseev, F. Alibart, D. Strukov, and S. V. Kalinin. *ACS Nano*, 6:7026, 2012.

[329] Q. N.Chen, Y. Ou, F. Ma, and J. Li. *Appl. Phys. Lett.*, 104:242907, 2014.

[330] V. Sundar and R. E. Newnham. *Ferroelectrics*, 135:431, 1992.

[331] G. da Cunha Rodrigues, P. Zelenovskiy, K. Romanyuk, S. Luchkin, Y. Kopelevich, and A. L. Kholkin. *Nat. Comm.*, 6:7572, 2015.

[332] S. Chandratre and S. Sharma. *Appl. Phys. Lett.*, 100:2013, 2012.

[333] M. T. Ong and E. J Reed. *ACS Nano*, 6:1387, 2012.

[334] M. T. Ong, K. A. N. Duerloo, and E. J. Reed. *J. Phys. Chem. C*, 117:3615, 2013.

[335] K. A. N. Duerloo, M. T. Ong, and E. J. Reed. *J. Phys. Chem. Lett.*, 3:2871, 2012.

[336] K. A. N. Duerloo and E. J. Reed. *Nano Lett.*, 13:1681, 2013.

[337] Z. Chang, W. Yan, J. Shang, and J. Z. Liu. *Appl. Phys. Lett.*, 105:023103, 2014.

[338] W. Wu, L. Wang, Y. Li, F. Zhang, L. Lin, S. Niu, D. Chenet, X. Zhang, Y. Hao, T. F. Heinz, J. Hone, and Z. L. Wang. *Nature*, 514:470, 2014.

[339] M. Zelisko, Y. Hanlumyuang, S. Yang, Y. Liu, C. Lei, J. Li, P. M. Ajayan, and P. Sharma. *Nat. Comm.*, 5:4284, 2014.

[340] S. V. Kalinin, S. Jesse, B. J. Rodriguez, Y. H. Chu, R. Ramesh, E. A. Eliseev, and A. N. Morozovska. *Phys. Rev. Lett.*, 100:155703, 2008.

[341] A. A. Bokov, B. J. Rodriguez, X. Zhao, J.-H. Ko, S. Jesse, X. Long, W. Qu, T. H. Kim, J. D. Budai, A. N. Morozovska, S. Kojima, X. Tan, S. V. Kalinin, and Z.-G. Ye. *Z. Kristallogr.*, 226:99–107, 2011.

[342] D. Denning, S. Alilat, S. Habelitz, A. Fertala, and B. J. Rodriguez. *J. Struct. Biol.*, 180:409, 2012.

[343] Y. Kim, X. Lu, S. Jesse, D. Hesse, M. Alexe, and S. V. Kalinin. *Adv. Funct. Mat.*, 23:3971, 2013.

[344] E. Strelcov, A. Belianinov, Y.-H. Hsieh, S. Jesse, A. P. Baddorf, Y.-H. Chu, and S. V. Kalinin. *ACS Nano*, 8:6449, 2014.

[345] R. K. Vasudevan, A. Tselev, A. P. Baddorf, and S. V. Kalinin. *ACS Nano*, 8:10899, 2014.